On the Attribution of Binding Energy in Antigen–Antibody Complexes McPC 603, D1.3, and HyHEL-5†

Jiri Novotny,*,‡,§ Robert E. Bruccoleri,‡,§ and Frederick A. Saul∥

Massachusetts General Hospital and Harvard Medical School, Boston, Massachusetts 02114, and Department of Immunology, Institut Pasteur, 75724 Paris Cedex 15, France

Received September 19, 1988; Revised Manuscript Received January 13, 1989

ABSTRACT: Using X-ray coordinates of antigen–antibody complexes McPC 603, D1.3, and HyHEL-5, we made semiquantitative estimates of Gibbs free energy changes (ΔG) accompanying noncovalent complex formation of the McPC 603 Fv fragment with phosphocholine and the D1.3 or HyHEL-5 Fv fragments with hen egg white lysozyme. Our empirical ΔG function, which implicitly incorporates solvent effects, has the following components: hydrophobic force, solvent-modified electrostatics, changes in side-chain conformational entropy, translational/overall rotational entropy changes, and the dilutional (cratic) entropy term. The calculated ΔG ranges matched the experimentally determined ΔG of McPC 603 and D1.3 complexes and overestimated it (i.e., gave a more negative value) in the case of HyHEL-5. Relative ΔG contributions of selected antibody residues, calculated for HyHEL-5 complexes, agreed with those determined independently in site-directed mutagenesis experiments. Analysis of ΔG attribution in all three complexes indicated that only a small number of amino acids probably contribute actively to binding energetics. These form a subset of the total antigen–antibody contact surface. In the antibodies, the bottom part of the antigen binding cavity dominated the energetics of binding whereas in lysozyme, the energetically most important residues defined small (2.5–3 nm^2) "energetic" epitopes. Thus, a concept of protein antigenicity emerges that involves the active, attractive contributions mediated by the energetic antigenic epitopes and the passive surface complementarity contributed by the surrounding contact area. The D1.3 energetic epitope of lysozyme involved Gly 22, Gly 117, and Gln 121; the HyHEL-5 epitope consisted of Arg 45 and Arg 68. These are also the essential antigenic residues determined experimentally. The above positions belong to the most protruding parts of the lysozyme surface, and their backbones are not exceptionally flexible. Least-squares analysis of six different antibody binding regions indicated that the geometry of the VH–VL interface β-barrel is well conserved, giving no indication of significant changes in domain–domain contacts upon complex formation.

Antibody molecules recognize their specific antigens with an exquisite specificity: that is, antibodies elicited in response to immunization with an antigen form tight noncovalent complexes with this antigen, but not with chemically related structures. Much work has been directed toward understanding the molecular basis of this specificity, definition and analysis of antigenic epitopes on surfaces of proteins, and similar relevant problems of immunological interest [see, e.g., Sela (1969), Benjamin et al. (1984), Tainer et al. (1985), and Berzofsky (1985) for reviews]. Recently, two X-ray crystallographic structures of monoclonal immunoglobulin Fab[1] fragments complexed with the protein hen egg white lysozyme became available [D1.3 (Amit et al., 1986) and HyHEL-5 (Sheriff et al., 1987)], thus making it possible to analyze specificity of these antibodies at the molecular level.

The above crystal structures revealed a close complementarity between antigen and antibody contact surfaces and established hydrogen-bond, van der Waals, and charge–charge interactions that determine the specificity of association (Mariuzza et al., 1987; Alzari et al., 1988; Davies et al., 1988). However, structural complexity of interatomic contacts is considerable, and our understanding of how to account for the energy contributed by different types of interactions remains inadequate. In fact, direct comparison of the X-ray structures with established immunological evidence seems to produce paradoxes. For example, results of competition experiments on polyclonal and monoclonal antibodies suggested that about four, or less, residues are sufficient to define an antigenic epitope (Kabat, 1970; Schechter, 1971; Hodges et al., 1988), yet the total contact area between the Fab and lysozyme involves some 10–15 amino acids on each side. Naive estimates of binding strength, which take into account the large contact areas (≈16 nm^2) and the number of hydrogen bonds made across the interface, suggest binding constant values far exceeding those derived from measurements. Accordingly, computational analysis of Gibbs free energy attribution becomes necessary. The conceptual complexity associated with protein–protein noncovalent complex formation requires, however, that we first formulate a "minimal", i.e., the simplest possible, empirical Gibbs free energy model and investigate its applicability to macromolecular complexes. If the model accounts qualitatively (or semiquantitatively) for the most important experimental observations, it is worth further refinement and application to a wider range of macromolecular systems. By repeated cycles of improvement, a more accurate

† Part of this work was carried out by J.N. while on leave of absence in France, and financial assistance from the French INSERM is gratefully acknowledged. This work was also supported by a grant from the Office of Naval Research to J.N.

* Address correspondence to this author.

‡ Massachusetts General Hospital and Harvard Medical School.

§ Present address: Squibb Institute for Medical Research, Princeton, NJ 08543-4000.

∥ Institut Pasteur.

[1] Abbreviations: Fab, antigen binding fragment of immunoglobulins; VL, light-chain variable domain; VH, heavy-chain variable domain; Fv, immunoglobulin fragment composed of the VL and VH domains; CL, light-chain constant domain; CH1, heavy-chain first constant domain; rms, root mean square.

0006-2960/89/0428-4735$01.50/0

and general model will eventually evolve.

The notion of binding specificity derives from comparison of association constants, K_{AS}, characterizing the reaction

$$\text{antigen} + \text{antibody} = \text{complex}$$

Molar concentrations of the three molecular species are measured at equilibrium, and the strength (specificity) of the complex is estimated from its relative concentration, i.e., the ratio K_{AS} = [complex]/[antibody][antigen]. Related expressions involve the dissociation constant, $K_{DS} = 1/K_{AS}$, affinity (K_{DS} expressed in molar units), and $pK_A = \log K_{AS}$. The experimentally measured K_{DS} relates to the Gibbs free energy of complex formation, ΔG, as $\Delta G = RT \log K_{DS}$ (R, the gas constant, is the product of the Boltzmann constant, k and the Avogadro constant, L: $R = 8.314$ kJ mol^{-1} K^{-1}; T is temperature in kelvin). Changes in the Gibbs free energy, a thermodynamic quantity, can in principle be obtained from atomic structures of all the molecules involved in the reaction, provided all the physical forces responsible for the complex formation are accurately known. Traditionally, the Gibbs energy is partitioned into two components, the enthalpy, H (the internal potential energy of the system), and the entropy, S (indicative of distribution of energy among all the different states available to the system): $\Delta G = \Delta H - T\Delta S$.

Ab initio evaluations of Gibbs free energy changes in biological reactions are possible only in special cases (Mezei & Beveridge, 1986; Rossky, 1986; McCammon et al., 1986; Pettitt & Karplus, 1985) and often require considerable investments of supercomputer time (Bash et al., 1987). Approximate estimates of Gibbs energy changes of reactions involving proteins were first attempted by Chothia and Janin (1975). They discovered that contact areas of protein–protein complexes may give good estimates of binding energies, although the concept of contact area as the only measure of Gibbs energy change is clearly an oversimplification. Thus, e.g., the areas of contact between trypsin and bovine pancreatic trypsin inhibitor (Huber et al., 1974) and between the immunoglobulin Fc fragment and fragment B of staphylococcal protein A (Deisenhofer, 1981) are identical (13.9 nm^2 in both cases), whereas affinities of these two complexes differ by at least 6 orders of magnitude (0.1 pmol in the case of the trypsin–trypsin inhibitor and $\approx \mu$mol or less in the case of the Fc fragment–fragment B).

Empirical "atomic solvation parameters" have been developed with the aim of allowing estimates of Gibbs free energy changes as sums of independent atomic contributions (Eisenberg & McLachlan, 1986; Ooi et al., 1987). This treatment often gives values in close agreement with experimental measurements, but the concept of a single atomic solvation parameter precludes partition of the Gibbs energy changes into terms such as the "hydrophobic force" (solvent entropy changes at solute–solvent interfaces), electrostatic solvent screening/polarization effects, or conformational entropy changes that accompany noncovalent complex formation. Nonetheless, resolution of Gibbs energy into its component physical forces plays an important role in understanding macromolecular processes, such as protein–protein complex formation or protein folding. With this in mind, we have begun to develop an empirical free energy potential (Bruccoleri et al., 1986) by introducing solvent effects indirectly into the in vacuo empirical force field of Levitt and Lifson (1969). This approach has been inspired by an earlier work of Rashin (1984) and offers practical advantages, since (1) the total potential energy of the system is expressed as the sum of pairwise atomic interactions and, as such, it is straightforward to calculate from crystallographic coordinates and (2) in vacuo empirical energy potentials are widely used in computer programs such as AMBER (Weiner & Kollman, 1981), CHARMM (Brooks et al., 1983), DISCOVER (Hagler, 1984), ECEPP (Nemethy & Scheraga, 1983), GROMOS (Berendsen et al., 1984), and PAKGGRAF (Katz & Levinthal, 1976).

In this paper, we apply our empirical free energy potential to the crystallographic structures of antigen–antibody complexes, showing that the model accounts, in a semiquantitative way, for the most essential experimental observations relating to protein antigenicity and antibody–antigen complex formation.

The Minimal Model of Gibbs Free Energy Attribution

The present model is a modification of our previous analysis of critical peptide length allowing spontaneous formation of α-helical coiled coils (Bruccoleri et al., 1986). Using the program CONGEN (Bruccoleri & Karplus, 1987) and the X-ray-derived atomic coordinates, we calculate Gibbs energy on the basis of additive empirical free energy terms. We then evaluate the difference, ΔG, of Gibbs energies between the noncovalent complex and its parts.

The Gibbs free energy of a reaction, ΔG, represents a balance between differences in enthalpies and entropies of reactants and reaction products. The most important enthalpic contributions include differences in covalent, hydrogen-bond, van der Waals, and electrostatic energies. The predominant entropic contributions involve changes in solvent entropy at the solvent–solute interface (i.e., the hydrophobic effect in aqueous solutions), loss of bond configurational entropy on attainment of compact structures, and the decrease in molecular translational entropy on complex formation.

In our case, no changes in covalent energy occur, and no protein conformational changes are assumed to occur upon complex formation. This second assumption is necessary initially, leading to estimates of Gibbs free energy changes associated with a "rigid body" model, the simplest possible concept of noncovalent complex formation. The possibility of a more complicated, dynamic model (Weber, 1975) is referred to future work. Strictly speaking, the Gibbs free energy of protein complexes is a time-averaged quantity whose value depends upon the fractions of time spent in different conformations and therefore upon protein dynamics (Xu & Weber, 1982). By formulating a minimal rigid body model, we assume that the *average*, "platonic" X-ray picture of proteins (Weber, 1975) accounts sufficiently well for the *average* thermodynamic properties of the system (such as K_{AS} measured at equilibrium).

In what follows, we give a brief summary of the components of our empirical Gibbs free energy potential, with short discussions.

Hydrophobic Effect, ΔG_Φ. Chothia (1974) showed that the free energy of transferring an amino acid side chain from water to a nonpolar solvent [the hydrophobic effect; cf. Kauzmann (1959) and Nozaki and Tanford (1971)] is directly proportional to the solvent-accessible surface of the side chains [see also Rose et al. (1985b)]; 1 Å^2 (0.01 nm^2) of buried surface corresponds to 104.5 J (25 cal) of hydrophobic stabilization. A direct experimental support for the proportionality between surface area and hydrophobic force has recently been obtained from stability measurements of single residue mutants (Matsumura et al., 1988) of the T4 phage lysozyme. Likewise, free energy perturbation calculations on amino acids in water (Bash et al., 1987) showed the total effect of embedding a nonpolar group in water to be the sum of the work needed to create a cavity in the solvent plus specific solvent–solute in-

teractions. Both these contributions scale with the solvent-accessible surface of the solute.

We use the algorithm of Lee and Richards (1971) to calculate solvent-accessible surfaces. The difference between solvent-accessible surfaces of free and complexed molecules gives the contact area of the complex. ΔG_Φ is then obtained as $\Delta G_\Phi = 104.5(\text{contact} - \text{area})$ (in joules).

Electrostatic Interactions and Hydrogen Bonds. The most rigorous treatment of electrostatic interactions in aqueous solutions involves solving the equations of the static electromagnetic field, such as the Poisson equation, for molecules imbedded in solution (Warwicker, 1986). It has recently been shown (Warshel et al., 1986; Gilson & Honig, 1987; Sternberg et al., 1987) that numerical solutions of the linearized Poisson equation exactly reproduce changes in titration curves (pK_H values of individual electrically charged groups) associated with single-residue mutations introduced into proteins. It has also been demonstrated that macroscopic electrostatic models which incorporate solvent effects indirectly (Rashin & Namboodiri, 1987), e.g., via a distance-dependent dielectric constant (Warshel & Levitt, 1976; Gelin & Karplus, 1979; Mehler & Eichele, 1984), reproduce the experimentally observed pK_H changes equally well (Sternberg et al., 1987). In our model, we employ the solvent-screened, macroscopic dielectric Coulomb potential

$$Q_iQ_j/(4\pi Kr_{ij}r_{ij}) \quad (1)$$

(Q_i and Q_j, atomic charges; r_{ij}, distance between atoms; the dielectric constant formally equals Kr_{ij}) to evaluate all the pairwise atomic interactions. Introduction of the constant K allows for adjustment of the calculated interactions to the expected values derived from numerical solution of the Poisson equation.

To gauge our electrostatic potential, we employed the model of calcium ion binding to bovine intestinal calcium-binding protein: in pilot calculations, we adjusted results obtained with eq 1 to agree with electrostatic binding energies of the two calcium ions evaluated by Gilson and Honig (1988b). We found, in accord with the previous work (Gilson & Honig, 1988a,b; Whitlow & Teeter, 1986), that setting the dielectric constant $D = r_{ij}$ leads to an overestimation of the total solvent-modified electrostatic forces. The correct value is obtained with $D = 4r_{ij}$ [cf. also Witlow and Teeter (1986)]. Thus, our formula for calculating protein electrostatic interactions in solution is $G_{EL} = \sum Q_iQ_j/(16\pi r_{ij}^2)$, where the sum is taken over all the possible atomic pairs. The desired $\Delta G_{EL} = (G_{EL})_{parts} - (G_{EL})_{complex}$.

We specifically note that the partial atomic charges and van der Waals radii used by us and by Gilson and Honig (Weiner et al., 1984; Singh & Kollman, 1984; Reiher, 1985) are to be preferred in solvent-modified electrostatic calculations, for the following reasons. First, the charges implicitly include polarization effects, such as those described by Quiocho et al. (1987) for peptide backbone oxygen and nitrogen atoms, by assigning appropriately higher point charges to all the polar atoms. Second, this parametrization was designed to reproduce hydrogen bonding as a solely electrostatic phenomenon, dispensing with the additional (and not quite accurate), geometric hydrogen-bonding term.

Although the absolute strength of a hydrogen bond is in the range of 25–42 kJ (6–10 kcal; Eisenberg & Kauzmann, 1969), protein–protein complex formation involves replacing hydrogen bonds that surface atoms make to water with protein–protein hydrogen bonds. The free energy difference associated with this process has been estimated to about −2 kJ (−0.5 kcal) for atoms without formal charges and to about −6 kJ (−1.5 kcal) and more for formally charged atoms (Fersht et al., 1985). The electrostatic model described here does indeed yield electrostatic difference values in this range (see below).

Changes in Conformational Entropy. Our rigid body model determines the ΔG value associated with the following thought experiment: the two molecules that make the crystallographic complex are translated away from each other, and it is assumed that their association (i.e., reversal of the translation) involved no structural changes with respect to the observed crystallographic structures. This concept does, however, imply immobilization of some residues and a concomitant loss of torsional degrees of freedom. Side chains at the interface area, originally free to choose among different rotational states of approximately equal energy, are forced to adopt the single conformation seen in the complex. The minimal estimate of conformational freedom lost assumes that each torsional degree of freedom has approximately three equienergetic states available, namely, the trans and ±gauche (Benedetti et al., 1983; James & Sielecki, 1983; Summers et al., 1987; McGregor et al., 1987; Ponder & Richards, 1987). To estimate the total loss of side-chain conformational entropy ΔS_{CF}, we use the atoms involved in the contact area of the complex to estimate the number, N, of side-chain torsions fixed; $\Delta S_{CF} = -R \log (3^N) = -NR \log 3$. This treatment leads to estimates whose range agrees with that of conformational entropy estimates deduced from temperature dependence of entropy of unfolding (Privalov, 1979). Note that for $N = 1$, the $-T\Delta S_{CF} = 2.7$ kJ (0.6 kcal) at 300 K; this is equal to the "1-kT" amount of thermal energy, or the energy content of 1 deg of freedom at temperature T, as given by the Maxwell–Boltzmann distribution law (Atkins, 1978).

The above-described procedure for estimating changes in conformational entropy is likely to give an underestimate. An extensive contact of two groups of bonded atoms probably restricts more than just one torsional degree of freedom. For example, van der Waals barriers encountered by a side-chain carboxyl group, as it enters into the complex, are likely not only to freeze the rotation of the carboxyl along the Cβ–Cγ bond but also to partially hinder the rotation of the adjacent Cα–Cβ bond. The number, N, of dihedral angles hindered in this situation would be greater than 1 but less than 2. Consequently, we employed a range of values $1.5 > N > 1$, instead of simply setting $N = 1$, whenever appropriate, with the result of obtaining a range of probable $-T\Delta S_{CF}$ values rather than a single number (in the above-mentioned example of the aspartate side chain, 1 would be the lowest estimate for N, and $N = 1.5$ would be the highest estimate). Admittedly, this approximation is somewhat subjective and gives only crude entropic estimates. In the future, more accurate estimates of restricted conformational space will be obtained by comparing results of uniform conformational sampling of side chains in the complex and in free molecules.

Changes in Translational and Overall Rotational Entropy. As the complex is formed, two independent molecules become tightly associated and the system as a whole becomes more ordered. That is, an amount of translational rotational entropy ΔS_{TR} has been lost. Accurate estimates of the amount $T\Delta S_{TR}$ are possible only for the gas phase, with use of the quantum mechanical Sakkur–Tetrode equation (Atkins, 1978). In solutions, the best available estimates are those of Page and Jencks (1971) and Jencks (1981), based on rate enhancements observed in monomolecular, compared to bimolecular, reactions. Page and Jencks (1971) give an estimated range of $T\Delta S_{TR} = 7$–11 kcal/mol (29–46 kJ/mol) for enzymatic reactions, and we use the median value of 9 kcal in our calcu-

lations. Note that the value of translational/rotational entropy loss chosen does not affect relative differences of ΔG calculated for different antibody–antigen complexes.

Cratic Entropy. Our calculations are carried out on molecular structures in their assumed standard state (i.e., nominal 1 M concentrations), while experimental measurements of equilibrium constants are performed in dilute, typically micromolar, solutions. The calculated ΔG values must therefore contain the appropriate term, $T\Delta S_{CR}$, describing the entropy difference associated with an approximately infinite dilution (cratic entropy). We use the estimate of ΔS_{CR} introduced by Kauzmann (1959): $\Delta S_{CR} = R \log (1/55.6)$, where the numeric constant, 55.6, is the molar concentration of pure water. The $T\Delta S_{CR}$ term then becomes $\approx$2 kcal ($\approx$8.4 kJ).

In summary, our Gibbs free energy model has the components

$$\Delta G = \Delta G_{\Phi} + \Delta G_{EL} - T\Delta S_{CF} - T\Delta S_{TR} - T\Delta S_{CR} \quad (2)$$

where

$$\Delta G_{\Phi} = 104.5(\text{contact} - \text{area}) \quad \text{(kJ)} \quad (3)$$

$$G_{EL} = \sum Q_i Q_j / 16\pi r_{ij}^2 \quad (4)$$

$$T\Delta S_{CF} = -RT \log (3^N) = -9.12N \quad \text{(kJ)} \quad (5)$$

$$T\Delta S_{TR} = 37.6 \quad \text{(kJ)} \quad (6)$$

$$T\Delta S_{CR} = RT \log (1/55.6) = 8.4 \quad \text{(kJ)} \quad (7)$$

(R, gas constant; Q_i, partial charge of the ith atom; r_{ij}, distance between the ith and jth atoms; N, number of torsional degrees of freedom constrained in the complex).

Methods of Computation

Atomic coordinates of the bovine intestinal calcium-binding protein (Szebenyi & Moffat, 1986), Fab fragments KOL (Marquart et al., 1980), NEW (Saul et al., 1978), and J539 (Suh et al., 1986), free McPC 603 Fab fragment (Satow et al., 1986), McPC 603 Fab fragment complexed with phosphocholine, and HyHEL-5 antibody Fab fragment complexed with lysozyme (Sheriff et al., 1987) were obtained from the Brookhaven Proten Data Bank (Bernstein et al., 1977); those of the D1.3 antibody Fab complex with lysozyme (Amit et al., 1986) were kindly provided by Roberto Poljak (Pasteur Institute, Paris). With the atomic coordinates, the structures were built in the computer by using the program CONGEN (Bruccoleri & Karplus, 1987), which incorporates many aspects of the program CHARMM (Brooks et al., 1983). For free energy calculations, only the Fv parts of the Fab fragments were considered; that is, the light- and heavy-chain constant domains CL and CH1 were deleted from the structures. Hydrogens attached to polar atoms were constructed explicitly by the program from internal coordinates. Aliphatic hydrogens were made parts of "extended" carbon atoms, by virtue of increased carbon van der Waals radii. For calculation of aromatic quadrupole effects (Burley & Petsko, 1985) aromatic hydrogens were constructed on aromatic rings and treated explicitly; partial atomic charges of 0.15e (Williams, 1980) were assigned to phenylalanine aromatic hydrogens and –0.15e to the corresponding aromatic carbons (e, the charge of proton, equals 1.602×10^{-19} C).

The parameters used in empirical energy calculations were essentially those described by Brooks et al. (1983), except for the partial atomic charge set and van der Waals radii, which followed the recommendations of Weiner et al. (1984), Singh and Kollman (1984), and Reiher (1985). The typical partial charge values are as follows: peptide oxygen and carbon, 0.55e and –0.55e, respectively; α carbon, peptide nitrogen and hydrogen, 0.10e, –0.35e, and 0.25e, respectively; asparagine γ carbon and oxygen, 0.55e and –0.55e, respectively; serine β carbon, γ oxygen, and γ hydrogen, 0.25e, –0.65e, and 0.4e, respectively; etc. Typical values of the van der Waals radii include the following: carbon, 2.100 Å (210 pm); extended carbon with one hydrogen, 2.365 Å; nitrogen and oxygen, 1.6 Å; hydrogen, 0.8 Å; charged hydrogen, 0.6 Å.

The parameters needed to construct the phosphocholine molecule were assembled from the known bond, bond angle, and partial atomic charges of its constituent atoms. Atoms involved in phosphoester linkage were assigned values of phosphodiester atom parameters from the DNA Residue Topology File (Brooks et al., 1983). At physiological pH, the ethyl phosphate group is expected to be doubly charged. The single hydrogen atom was introduced on the O3 atom on the basis of (1) a comparison of P–O1, P–O2, P–O3, and P–O4 bond lengths and (2) the outward-oriented position of the O3 atom (cf. the Brookhaven Protein Data Bank entry for phosphocholine atom nomenclature).

After polar hydrogens were introduced into the crystallographic structures, the structures were energy minimized by using the 200 cycles of the ABNR (adopted basis Newton–Raphson) protocol (Brooks et al., 1983) with harmonic constraints of 20 kcal (83.6 kJ) applied to all the atoms. The purpose of the minimization was to relieve any accidental atomic overlaps and improve on the geometry of the structure, with respect to the van der Waals radii and covalent parameters used by the program CONGEN. For energy minimization, no explicit hydrogen-bonding term was used (i.e., the hydrogen bonds were treated strictly electrostatically), and a cutoff distance of 0.8 nm was imposed to evaluations of noncovalent interactions. Energy minimization was accompanied by large decrease in empirical potential energy, particularly its van der Waals term, but only minute atomic displacements with respect to the original X-ray-derived positions: the average rms shift between the crystallographic and the energy-minimized structures was 0.3 Å (30 pm).

To evaluate Gibbs free energy contributions, calculations of solvent-accessible surfaces and electrostatic energies were carried out. In electrostatic calculations, all atomic pair interactions were evaluated; that is, no cutoff distance was employed. The values were calculated on the complexes first and then on the Fv fragments and the antigens separately, the antigen and antibodies being translated away from each other over the distance of 100 nm (1000 Å). Values listed are those obtained from difference tables of the ANALYSIS facility of the CONGEN program. To facilitate analysis of hydrogen bonding, tables of hydrogen-bond distances and angles were constructed as well.

Black-and-white, color-coded, space-filling, and line images of molecules and surfaces were produced by the CONGEN program, with the PLT2 (R.E.B. and D. States, personal communication) and Unified Graphics (Robert C. Beach, S.L.A.C. Computation Research Group, and R.E.B.) subroutines.

Least-squares superposition of selected pairs of atoms within the crystallographic structures was performed by the CONGEN program as previously described (Novotny & Haber, 1985). Likewise, the least-squares fitting of the twisted hyperboloid surface into the backbone atoms of β-sheets, using the formula

$$\frac{(x \cos Dz + y \sin Dz)^2}{A^2} + \frac{(-x \sin Dy + y \cos Dz)^2}{B^2} - \frac{z^2}{C^2} = 1 \quad (8)$$

Table I: Experimental and Calculated Gibbs Free Energies (kcal)

Gibbs free energy component	McPC 603 and phosphocholine	D1.3 and lysozyme	HyHEL-5 and lysozyme
ΔG measured	−6.6	−11.4	−14.2 ± 1
ΔG computed	−9 ± 3	−9 ± 3	−32 ± 5
ΔG_Φ	−10	−41	−47
ΔG_{EL}	−24	−21	−39
$-T\Delta S_{CF}$	14 ± 3	42 ± 3	43 ± 5
$-T\Delta S_{TR}$	9	9	9
$-T\Delta S_{CR}$	2	2	2

(x, y, and z, Cartesian atomic coordinates; A and B, major and minor semiaxes of elliptical cross section; C, hyperboloid curvature; D, pitch of the hyperboloid twist), was carried out as described (Novotny et al., 1984; Novotny & Haber, 1985).

Results and Discussion

In what follows, we first compare the calculated Gibbs energy differences of three antigen–antibody complexes, McPC 603, D1.3, and HyHEL-5, with the respective experimental values. We analyze the significance of values obtained for the individual composite terms, i.e., the hydrophobic effects, solvent-modified electrostatics, and losses of conformational entropy. Next, we analyze Gibbs energy contributions from VH and VL domains and their amino acid residues. Results of this analysis are then used to determine both the validity and limitations of our free energy model. Finally, we compare our data with known facts of the antigenicity of the lysozyme.

Table I lists the calculated and experimentally derived Gibbs energy changes of complex formations for all the crystal structures studied. The experimental values were obtained from Rudikoff et al. (1972) and Skerra and Plueckthurn (1988) (McPC 603–phosphocholine affinity 17 μmol), Verhoeyen et al. (1988) and the Pasteur group (D1.3–lysozyme affinity about 5 nmol; the value originally reported by Amit et al., 17 μmol, is now known to be incorrect), and Lavoie et al. (1989) (HyHEL-5–lysozyme affinity about 1 nmol). Our calculations produce a range of energies that include the experimental values in the case of McPC 603 and D1.3 but give a lower Gibbs energy change estimate in the case of HyHEL-5. However, the experimentally measured affinity of the HyHEL-5 complex is known to represent the most conservative estimate, and the actual affinity may be higher, perhaps approaching the calculated value. Alternative possible sources of disagreement are (1) part of the calculated Gibbs free energy difference in expended on inducing conformational changes in the antigen and/or antibody, (2) the calculated ΔG is accurate, and the excess of Gibbs free energy becomes dissipated against the steep van der Waals barriers of close atom–atom interactions, (3) our electrostatic calculations overestimate the strength of very close charge–charge interactions, and (4) a combination of some, or all, above-mentioned effects takes place.

In all three complexes, the productive (negative) and unfavorable (positive) entropic contributions (ΔG_Φ and $T\Delta S_{CF}$) are approximately equal, thus effectively canceling large parts of total entropic changes (Tables I and II). This situation was to be expected. Noncovalent biological reactions are characterized by entropy–enthalpy compensation (Lumry & Biltonen, 1969) and often are entropy-driven at low temperatures but enthalpy-driven at high temperatures (Mukkur, 1984; Ross & Subramanian, 1981). For this compensation to be generally possible, the opposing entropic contributions (increase in solvent entropy, decrease in side-chain configurational entropy) must approximately balance each other, leaving only a margin commensurable with solvent-screened electrostatic interactions, minus the translational/rotational and cratic term.

Table II: Contributions of VH and VL Domains to Antigen Binding (kcal)

ΔG component	McPC 603		D1.3		HyHEL-5	
	VH	VL	VH	VL	VH	VL
ΔG_Φ	−1.6	−1.1	−11.3	−9	−13.1	−10
$-T\Delta S_{CF}$	+4.3	+4.5	+9.0	+7.8	+12.6	+9.0
ΔG_{EL}	−10.2	−1.8	−9.1	−1.3	−16.7	−3.1
total ΔG	−7.5	+1.5	−11.4	−2.5	−17.2	−4.1

In Table II, relative contributions of the light- and heavy-chain variable domains (VL and VH) toward Gibbs energy differences are given. Interestingly, the heavy-chain contribution dominates complex formation in all three antibodies. This phenomenon may be related to two structural peculiarities: (1) heavy-chain hypervariable loops often contribute larger surface to the binding site than the light-chain loops do (Poljak et al., 1973); (2) the H2 and H3 loops, and particularly the peptide chain segment coded for by the D gene, are rich in electrically charged side chains, with an increased opportunity to establish favorable charge–charge interactions with the antigen.

Overall, our ΔG estimates indicate stable complex formation in all three cases studied and give acceptable absolute ΔG values for the McPC 603 and D1.3 complexes. Overestimation of the strength of the HyHEL-5 complex with lysozyme, on the other hand, points toward the necessity of future refinements in our free energy model. Nevertheless, our calculations appear to approximate well the expected relative contributions of electrostatic and entropic effects. In the following paragraphs, we proceed to a more detailed analysis of the ΔG attribution in the individual X-ray structures.

McPC 603 Fv Fragment and Phosphocholine. The crystallographic structure of the McPC 603 Fab fragment with its ligand phosphocholine represents an important test case of our Gibbs free energy model, inasmuch as (1) the crystallographic structure of the free, unliganded McPC 603 Fab is available, (2) the free and the liganded McPC 603 Fab fragments are essentially identical (total rms shift between the two structures is 0.3 Å), thus directly justifying the rigid body model of antibody–antigen complex formation in this particular case, (3) the conformational entropy of the phosphocholine is particularly simple to evaluate, and (4) the experimental ΔG value has been accurately determined by two independent groups (Rudikoff et al., 1972; Skerra & Plueckthurn, 1988).

Figure 1 highlights antibody side chains that make most important contacts with phosphocholine, based both on previously published analyses (Segal et al., 1974; Padlan et al., 1976) and on contact area values calculated by us. The phosphocholine backbone is seen adopting comfortably staggered conformations, with the P–O2–C1–C2 torsion ≈ +gauche and the O2–C1–C2–N torsion ≈ trans. In the antibody, the dominant ligand-contacting position of Arg H52 and Trp H107 is well apparent (0.23-nm^2, or 23-Å^2, contact surface in both residues). Residues Tyr H33 (0.11-nm^2 contact area), His L98 (0.13-nm^2 contact area), Ser L99 (0.09-nm^2 contact area), and Tyr L100 (0.18-nm^2 contact area) also make important contacts. Note that Trp H107 contacts the positively charged trimethylammonium group by its (partially negatively charged) ring face, while the two tyrosine rings H33 and L100 interact with the negatively charged phosphate group by their (partially positively charged) ring edges. To estimate the additional electrostatic stabilization arising from this arrangement, we recalculated the ΔG_{EL} term on the complex with all the protein aromatic hydrogens explicitly present,

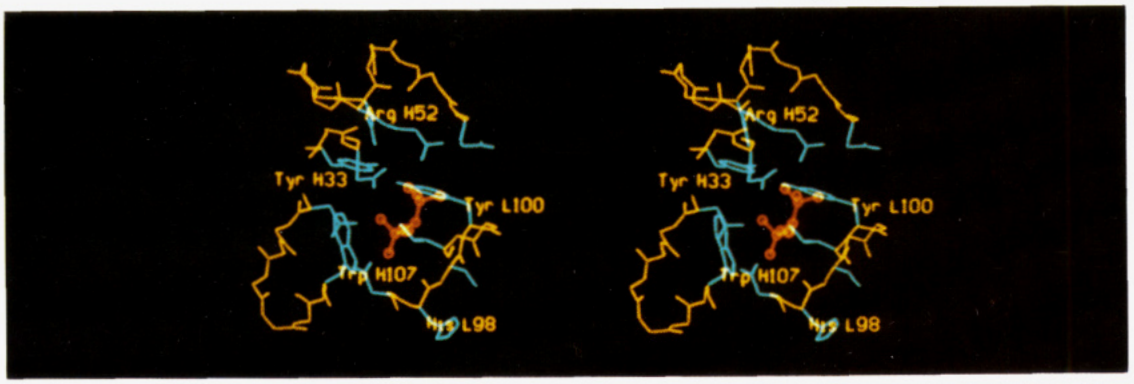

FIGURE 1: Stereo image of the McPC 603 combining site (yellow) with phosphocholine (red). Only the most important antigen-contacting residues are drawn. The trimethylammonium group of phosphocholine is at the bottom; the phosphate group is at the top.

Table III: Residue Contributions to Binding Energy: McPC 603 Antibody

residue	ΔG_Φ surface (Å²)	ΔG_Φ energy (kcal)	N	$-T\Delta S$ energy (kcal)	ΔG_{EL} energy (kcal)	total energy (kcal)
VH						
Arg 52	**22.8**	**−0.6**	**1**	**+0.7**	**−12**	**−12**
Trp 107[a]	22.9	−0.6	1	+0.6	0	0
Asn 56	3.1	0	1	+0.6	−0.3	+0.3
Glu 61	1.0	0	1	+0.6	+1.3	+0.6
Asn 101	0.8	0	1	+0.6	+0.1	+0.7
Tyr 33	11.4	−0.3	2	+1.3	+1.3	+2.3
VL						
Asp 97	**1.9**	**0**	**1**	**+0.6**	**−1.1**	**−0.5**
His 98	12.8	−0.3	1	+0.6	−0.4	−0.1
Ser 99	9.0	−0.2	1	+0.6	−0.2	+0.2
Phe 38	0.7	0	1	+0.6	0	+0.6
Tyr 100[a]	18.5	−0.5	2	+1.3	0	+0.6
Leu 102	1.5	0	1	+0.6	0	+0.6

[a] The electrostatic energy interaction values calculated with all aromatic hydrogens present ($Q_H = 0.15e$) are Trp 107, −0.3 kcal, and Tyr 100, −0.9 kcal. N, number of torsions constrained in the complex.

regenerating the quadrupole moments of the rings via partial point charges (≈0.15e) assigned to the C and H atoms. We obtained about −1 kJ additional electrostatic energy in the case of Trp H107 and ≈−4 kJ (−1 kcal) in the case of Tyr L100.

Table III lists the most important amino acid residue contributions toward the Gibbs energy of McPC 603 complex formation. The final Gibbs energy difference is a balance of "repulsive" and "attractive" contributions, with that of Arg H52 predominating by a large margin over the sum total of all the other residues. The role of the guanidinium group of the arginine side chain thus appears to be truly "energetic", while the other residues contribute to the binding affinity mostly indirectly, by providing shape complementarity either via their surfaces or by establishing directional hydrogen bonds that keep the important side chains "in place". This impression seems to be supported by the following observations. First, in the ligand-free McPC 603 antibody the position reserved for the phosphate moiety is occupied by a sulfate ion (Satow et al., 1986), suggesting that the electrostatic field created by the Arg H52 is strong enough to attract and immobilize nonspecific counterions. Second, chemical modification of arginine side chains, in phosphocholine-binding antibodies homologous to McPC 603 (such as H8; Grossberg et al., 1974), totally abolishes ligand binding. Chemical modifications of aspartate, glutamate, or lysine side chains have a more moderate effect, with residual affinity toward phosphocholine persisting even after the modification.

D1.3 Fv Fragment and Lysozyme. Figure 2 depicts all the important contact residues in both protein moieties of the

Table IV: Residue Contributions to Binding Energy: D1.3 Antibody

residue	ΔG_Φ surface (Å²)	ΔG_Φ energy (kcal)	N	$-T\Delta S$ energy (kcal)	ΔG_{EL} energy (kcal)	total energy (kcal)
VH						
Asp 100	**60.4**	**−1.5**	**2**	**+1.3**	**−3.7**	**−3.9**
Gly 31	**51.3**	**−1.3**	**0**	**0**	**−0.5**	**−1.8**
Tyr 101	**72.4**	**−1.8**	**2**	**1.3**	**−1.1**	**−1.6**
Arg 99	**61.2**	**−1.5**	**2.5**	**+1.6**	**−1.4**	**−1.3**
Trp 52	**61.7**	**−1.5**	**1**	**+0.6**	**−0.2**	**−1.1**
Gly 53	**11.1**	**−0.3**	**0**	**0**	**−0.7**	**−0.9**
Thr 30	43.1	−1.1	3	+2.0	−1.1	−0.2
Tyr 32	27.6	−0.7	2	+1.3	−0.4	+0.2
Leu 29	28	−0.7	2	+1.3	0	+0.6
Arg 97	0	0	0	0	+0.7	+0.7
VL						
Tyr 50	**73.8**	**−1.8**	**2**	**+1.3**	**−1.3**	**−1.8**
His 30	**75.3**	**−1.9**	**1**	**+0.6**	**+0.1**	**−1.2**
Trp 92	**58.5**	**−1.5**	**1**	**+0.6**	**−0.1**	**−1.0**
Thr 53	19	−0.5	3	+2.0	0	+1.5

Table V: Residue Contributions to Binding Energy: D1.3 Lysozyme

residue	ΔG_Φ surface (Å²)	ΔG_Φ energy (kcal)	N	$-T\Delta S$ energy (kcal)	ΔG_{EL} energy (kcal)	total energy (kcal)
Gly 22	**57.9**	**−1.5**	**0**	**0**	**−2.5**	**−4.0**
Gly 117	**79.8**	**−2.0**	**0**	**0**	**−1.1**	**−3.1**
Gln 121	**117.4**	**−2.9**	**2.5**	**+2.0**	**−1.3**	**−2.2**
Ser 24	54.3	−1.4	2	+1.3	−1.5	−1.6
Asp 18	27	−0.7	1.5	+0.8	−1.5	−1.4
Asn 19	79.2	−2.0	2	+1.3	−0.3	−1.0
Ile 124	40	−1.0	2.5	+1.8	0	+0.8
Lys 13	10	−0.3	1	+1.3	−0.1	+0.9
Asn 113	13.5	−0.3	2	+1.3	0	+1.0
Arg 125	43.5	−1.1	5	+2.6	0	+1.5
Leu 129	32.4	−0.8	5	+2.6	0	+1.8

complex (Amit et al., 1986). The lysozyme side chain Gln 121 penetrates the deepest into the antibody binding site and is surrounded by aromatic rings of antibody side chains Tyr H101, Tyr L50, and Trp L92. Tables IV and V list the most important residue contributions to Gibbs energy of complex formation. A noteworthy feature of both the tables is the fact that a small number of residues account for most of the calculated ΔG. In the VH domain, the segment Arg-Asp-Tyr (H99–H101) alone contributes some −30 kJ (≈−7 kcal) of binding free energy. VL domain contributions are divided more evenly among all the three hypervariable loops. In Figure 3 the amino acids of the binding site, as listed in Table IV, have been color coded according to their ΔG contributions. The binding site appears in this representation as a patchwork of positive and negative contributions. A large part of the binding affinity can be envisioned as originating from the deepest part of the binding site, with an area significantly

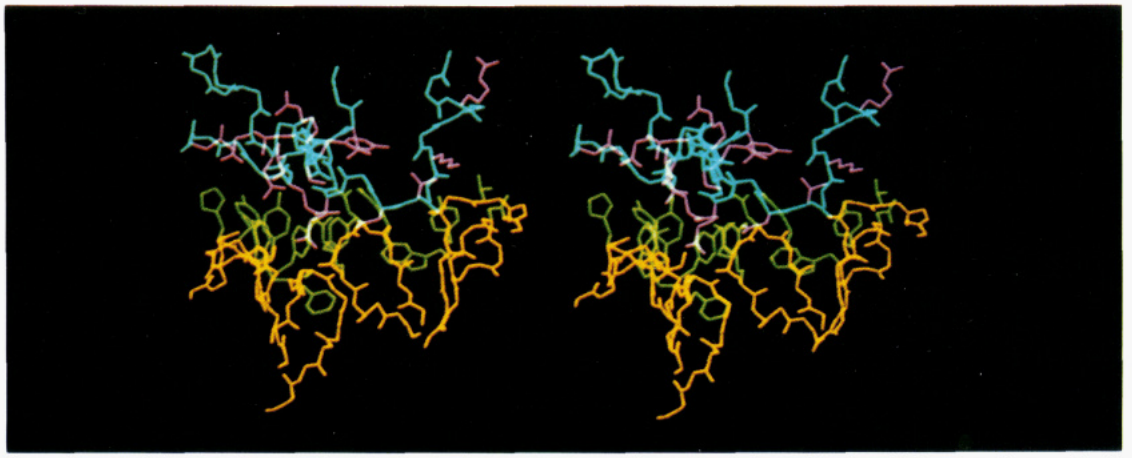

FIGURE 2: Stereo image of the D1.3 binding site with parts of the lysozyme surface. The color coding is as follows: yellow, antibody backbone; green, antibody side chains; cyan, lysozyme backbone; magenta, lysozyme side chains.

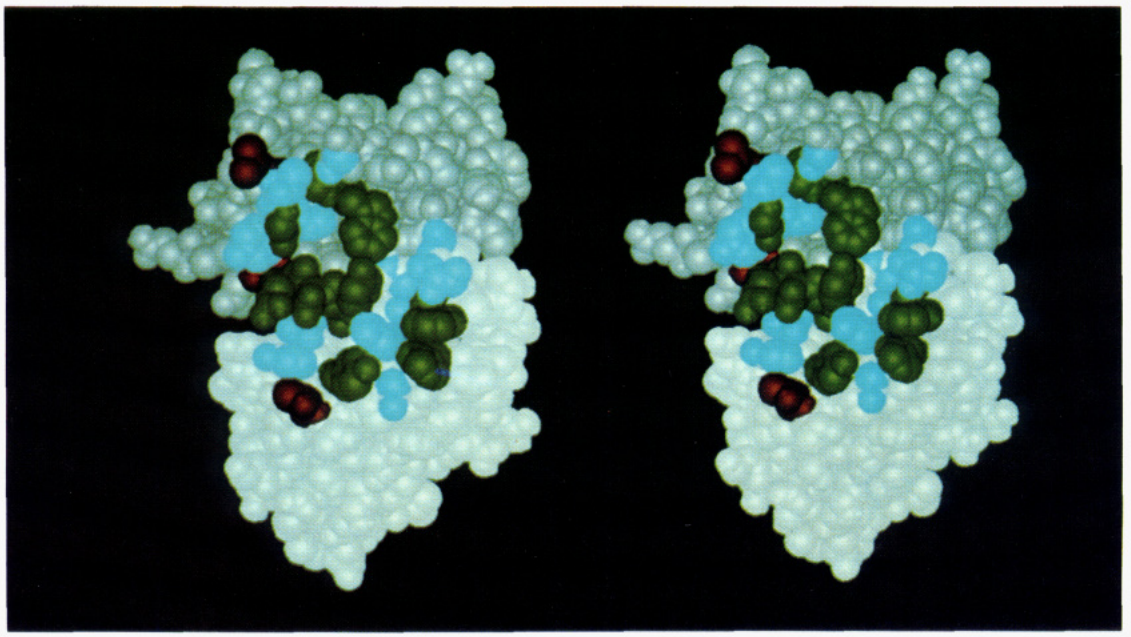

FIGURE 3: Stereo image of the surface of the D1.3 antibody binding site. The heavy chain is in dark grey; the light chain is in light gray. Residues (or selected, contact-making atoms thereof) involved in contacts with the lysozyme are color coded in accordance with values listed in Table IV as follows: green (strong binding contributions), heavy-chain residues Gly 31, Trp 52, Gly 53, Arg 99, Asp 100, and Tyr 101 and light-chain residues His 30, Tyr 50, and Trp 92; sky blue (neutral contributions, 0.6 kcal > ΔG > −0.9 kcal), heavy-chain residues Tyr 32, Gly 33, Asp 54, and Arg 102 and light-chain residues Asn 31, Tyr 32, Tyr 49, Phe 91, Trp 92, Ser 93, Thr 94, and Arg 96; red (free energy contributions opposing binding), heavy-chain residues Leu 29 and Arg 97 and light-chain residue Thr 53.

smaller (≈65%) than the whole antibody–lysozyme contact surface.

Verhoeyen et al. (1988), using genetic engineering methods, grafted the three hypervariable loops of the D1.3 antibody heavy chain onto a different β-sheet framework (myeloma protein NEW) and showed that the hybrid heavy chain combines with the D1.3 light chain to produce an anti-lysozyme antibody with affinity comparable to that of the intact D1.3. They commented on the fact that Tyr H32 of the D1.3 H1 loop is devoid of important van der Waals contacts when surrounded by the NEW framework and hypothesize that a conformational change may be needed to restore the D1.3-like conformation of this side chain. It is interesting to note, in the context of their experiment, that Tyr H32 does not contribute significantly to the ΔG of the lysozyme–D1.3 complex according to our calculations (cf. Table IV).

The data reported in Table V amount to an energetic definition of the D1.3 antigenic epitope on the lysozyme surface. The energetic epitope consists of no more than five residues, Gly 22, Gly 117, and Gln 121 being much more important than the remaining two, Ser 24 and Asp 18. The size of this epitope corresponds well with that given, e.g., by Kabat (1970) or reported recently by Hodges et al. (1988), i.e., four residues or less. Figure 4 shows that residues 22, 117, and 121 belong among the most protruding parts of the lysozyme surface. Our calculated residue contributions to binding affinities are in agreement with the relative importance of individual side chains for antibody binding, as deduced from competition studies with homologous avian lysozymes (Amit et al., 1986; Harper et al., 1987). Specifically, Gln 121 is known to be essential for D1.3 antibody binding, as its replacement with His, Arg, or Asn leads to a significant loss of affinity. Glycines 22 and 117, having no side chains, are not amenable to comparative side-chain replacement experiments, and their involvement in the antibody binding would be difficult to detect by this method. Interestingly, Table V allows predictions that replacements of Asn 113, Arg 125, and Leu 129 with shorter side chains should improve on the affinity.

Table VI lists the most important hydrogen bonds spanning the antigen–antibody interface, similar to the analysis pub-

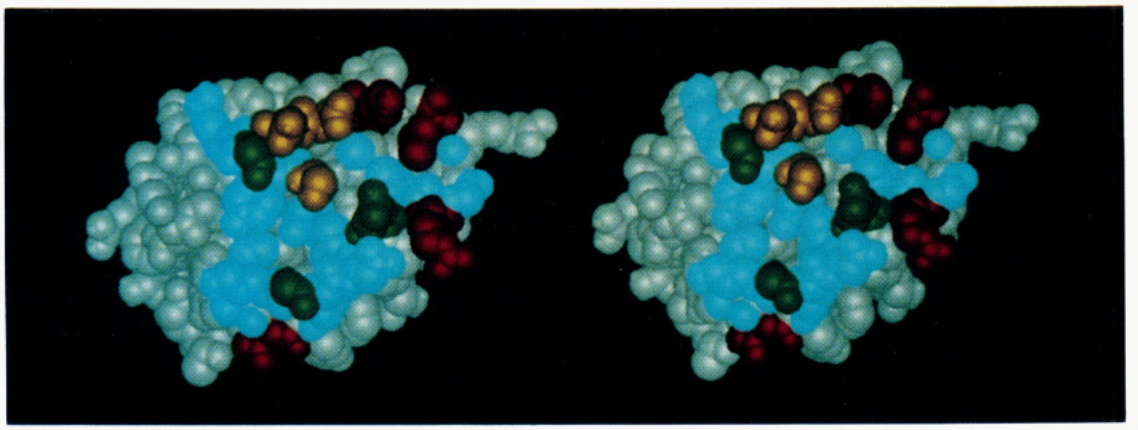

FIGURE 4: Stereo image of the lysozyme surface contacting the D1.3 antibody. Residues (or selected, contact-making atoms thereof) involved in contacts with the antibody are color coded in accordance with values listed in Table V as follows: green (strong binding contributions), Gly 22, Gly 117, and Gln 121; yellow (moderate binding contributions, $\Delta G < -2$ kcal), Ser 24, Asp 18, and Asn 19; sky blue (neutral contributions, 0.9 kcal $> \Delta G > -1$ kcal), Arg 21, Leu 25, Asn 27, Trp 111, Arg 112, Lys 116, Ile 124, Gly 126, and Cys 127; red (free energy contributions opposing binding), Lys 13, Asn 113, Arg 125, and Leu 129.

Table VI: Important Hydrogen Bonds between D1.3 Antibody and Lysozyme

hydrogen bond					
lysozyme atom	antibody atom	distance (Å)	angle (deg)	ΔG_{EL}[a] (kcal) atom 1	atom 2
(Asp 18) OD1	(Tyr L50) OH	2.9	19.8	−1.3	−1.2
(Asp 18) OD2	(Tyr L50) OH	4.2	25.9	−0.4	−1.2
(Gly 22) O	(Arg H99) NH1	2.7	42.0	−2.1	−1
(Gly 22) O	(Arg H102) NH1	3.2	19.0	−2.5	−0.6
(Ser 24) OG	(Asp H100) OD1	2.8	31.5	−0.9	−2.9
(Ser 24) OG	(Asp H100) OD2	3.3	30.7	−0.9	−1.8
(Asn 27) ND2	(Asp H100) OD1	3.0	20.2	−0.7	−2.9
(Lys 116) O	(Thr H30) OG1	2.7	38.5	−1.6	−0.7
(Lys 116) O	(Gly H31) N	2.7	39.0	−1.6	−0.6
(Gly 117) O	(Gly H53) N	2.8	28.9	−0.9	−0.5
(Asp 119) OD1	(Tyr H101) OH	3.5	61.2	+0.3	−1.2
(Gln 121) N	(Tyr H101) OH	2.9	18.4	−0.4	−1.2
(Gln 121) NE2	(Phe L91) O	2.7	0.8	−0.8	−0.9

[a] Electrostatic energies listed for hydrogen bond donor groups (e.g., N–H, H11–NH1–H12, etc.) are sums for all atoms of the group. Energy listed for carbonyl oxygen is the sum of contributions by atoms C and O.

Table VII: Residue Contributions to ΔG: HyHEL-5 Antibody

	ΔG_Φ		$-T\Delta S$		ΔG_{EL}	total
residue	surface (Å²)	energy (kcal)	N	energy (kcal)	energy (kcal)	energy (kcal)
VH						
Glu 50	**22.6**	**−0.6**	**3**	**+1.8**	**−9.2**	**−8.0**
Glu 35	**0.1**	**0**	**0.5**	**+0.3**	**−3.6**	**−3.3**
Trp 33	**84.8**	**−2.1**	**1**	**+0.6**	**−0.9**	**−2.4**
Asn 59	**58.5**	**−1.5**	**2**	**+1.3**	**−1.4**	**−1.6**
Tyr 101	87	−2.2	2	+1.3	−0.3	−1.2
Asp 31	31.7	−0.8	1	+0.6	−0.7	−0.9
Ser 55	65.8	−1.6	2	+1.3	−0.3	−0.6
Asn 100	15.7	−0.4	2	+1.3	−0.3	+0.6
Leu 52	28	−0.7	4	+2.2	0	+1.5
VL						
Arg 92	**127.8**	**−3.2**	**4.5**	**+2.6**	**−3.2**	**−3.8**
Trp 90	**84.5**	**−2.1**	**1**	**+0.6**	**0**	**−1.5**
Gly 91	**41.9**	**−1.0**	**0**	**0**	**−0.4**	**−1.4**
Tyr 31	66.2	−1.7	2	+1.3	0	−0.4
Tyr 33	14.4	−0.4	2	1.3	0	+0.9
Val 29	8.5	−0.2	2	+1.3	0	+1.1

Table VIII: Residue Contributions to ΔG: HyHEL-5 Lysozyme

	ΔG_Φ		$-T\Delta S$		ΔG_{EL}	total
residue	surface (Å²)	energy (kcal)	N	energy (kcal)	energy (kcal)	energy (kcal)
Arg 68	**136.7**	**−3.4**	**5**	**+2.6**	**−9.3**	**−10.1**
Arg 45	**162.9**	**−4.1**	**5**	**+2.6**	**−6.3**	**−7.8**
Pro 70	90.1	−2.3	0	0	−0.1	−2.2
Thr 43	74.6	−1.9	3	+2.0	−1.2	−1.1
Gly 67	52.5	−1.3	0	0	−0.3	−1.6
Thr 51	4.5	−0.1	0.5	+0.3	+0.3	+0.5
Asn 44	21	−0.5	2	+1.3	−0.2	+0.6
Asp 66	23.3	−0.6	1	+0.6	+1.4	+1.4

lished previously by Amit et al. (1986). It is worth noting, however, that the calculated strengths of hydrogen bonds are well within the range of expected ΔG values associated with exchanges of protein–water H-bonds for protein–protein H-bonds (Fersht et al., 1985). Thus, e.g., each of the two hydrogen bonds made by the (formally uncharged) side-chain oxygen atom of lysozyme residue 24 contributes some −2 kJ (−0.5 kcal) of electrostatic stabilization, whereas electrostatic stabilization calculated for hydrogen-bonded formally charged atoms (e.g., carboxylate oxygens of antibody residue H100) amounts to about −8 kJ (−2 kcal) and less. Relatively large electrostatic contributions associated with H-bonded peptide oxygens and nitrogens are due to the higher partial charges employed here and seem to model more realistically the additional electrostatic polarization often found in hydrogen-bonded peptide units (Quiocho et al., 1987).

HyHEL-5 Fv Fragment with Lysozyme. Figure 5 is a schematic representation of the antigen–antibody interface in this complex (Sheriff et al., 1987). The charge–charge, hydrogen-bonding interaction of the two arginine side chains, lysozyme residues 45 and 68, and the two glutamates, antibody residues H35 and H50, is particularly conspicuous. Tables VII–IX list all the important ΔG contributions in both protein moieties and the most important hydrogen bonds made across the interface, respectively. In addition to the four above-mentioned charged residues, the antibody side chain Arg L92 contributes some −16 kJ (−3.8 kcal) of Gibbs free energy stabilization (see the upper left center of Figure 5). A pictorial representation of the antibody binding site surface and residue contributions toward binding affinity (Figure 6) gives an im-

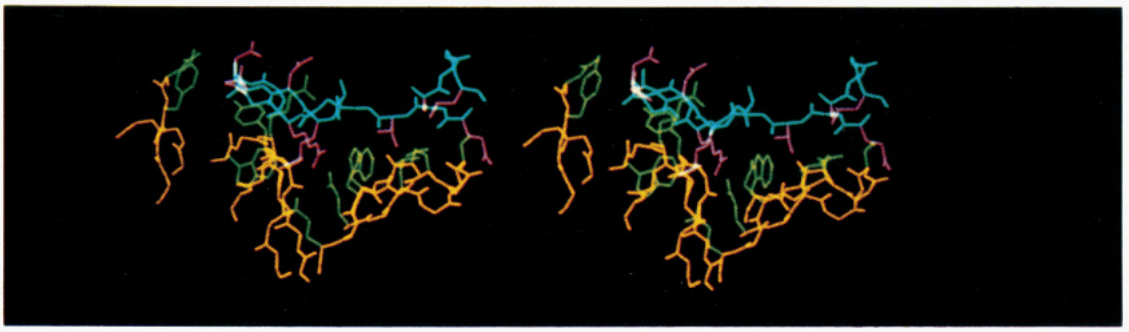

FIGURE 5: Stereo image of the HyHEL-5 binding site with parts of the lysozyme surface. The color coding is as follows: yellow, antibody backbone; green, antibody side chains; cyan, lysozyme backbone; magenta, lysozyme side chains.

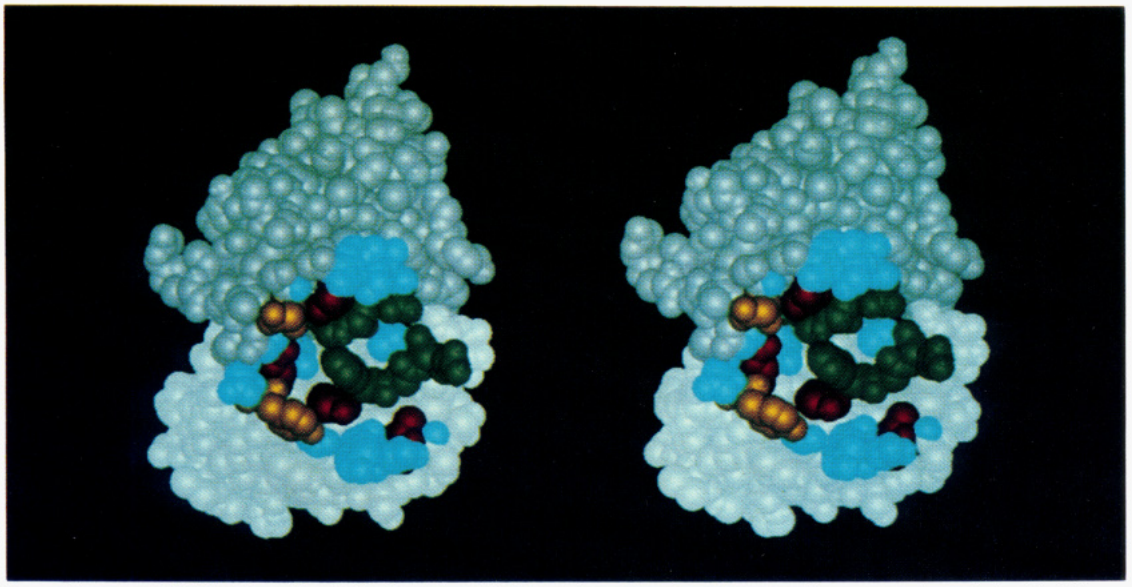

FIGURE 6: Stereo image of HyHEL-5 antibody binding site. Residues (or selected, contact-making atoms thereof) involved in contacts with the lysozyme are color coded in accordance with values listed in Table VII as follows: green (strong binding contributions), heavy-chain residues Trp 33, Glu 35, Glu 50, and Asn 59 and light-chain residues Gly 91, Arg 92, and Trp 90; yellow (moderate binding contributions, $\Delta G \approx -1$ kcal), heavy-chain residues Asp 31 and Tyr 101; sky blue (neutral contributions, 0.5 kcal $> \Delta G > -0.9$ kcal), heavy-chain residues Ser 30, Tyr 32, Trp 47, Ser 55, Gly 99, and Asp 102 and light-chain residues Ser 28, Asn 30, Tyr 31, Asp 49, and Pro 94; red (free energy contributions opposing binding), heavy-chain residues Leu 52 and Asn 100 and light-chain residues Val 29 and Tyr 33.

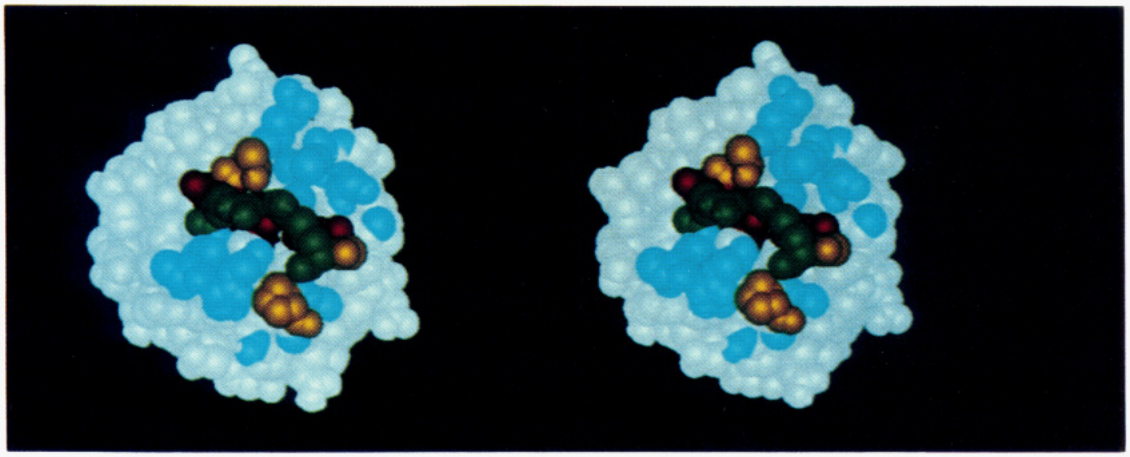

FIGURE 7: Stereo image of the lysozyme surface contacting the HyHEL-5 antibody. Residues (or selected, contact-making atoms thereof) involved in contacts with the antibody are color coded in accordance with values listed in Table VIII as follows: green (strong binding contributions), Arg 45 and Arg 68; yellow (moderate binding contributions, $\Delta G \approx -1$ to -2 kcal), Thr 43, Gly 67, and Pro 70; sky blue (neutral contributions), Gln 41, Asn 46, Thr 47, Asp 48, Gly 49, Arg 61, Thr 69, Gly 71, Ser 72, Pro 79, Ser 81, Leu 85, and Ser 85; red (free energy contributions opposing binding, $\Delta G > 0.4$ kcal), Asn 44, Thr 51, and Asp 66.

pression similar to that of the D1.3 antibody (Figure 3), namely, the most important side chains being clustered at the bottom of the binding site.

Results presented in Table VIII concur with experimental determination of residue Arg 68 as the essential one in the lysozyme epitope (Smith-Gill et al., 1982). Kam-Morgan and Smith-Gill (personal communication) recently measured relative affinities of lysozyme mutants Arg 45 → Lys and Arg 68 → Lys for the HyHEL-5 antibody. The mutation at position 45 lowers affinity about 1 order of magnitude, while the mutation at position 68 lowers affinity 3–4 orders of magnitude. These measurements give support to the calculated

Table IX: Important Hydrogen Bonds between HyHEL-5 Antibody and Lysozyme

hydrogen bond				ΔG_{EL}[a] (kcal)	
lysozyme atom	antibody atom	distance (Å)	angle (deg)	atom 1	atom 2
(Thr 43) OG1	(Asn H59) OD1	2.7	34.2	−0.7	−2
(Thr 43) OG1	(Asn H59) ND2	3.3	44.9	−0.7	−0.4
(Thr 43) O	(Asn H59) ND2	2.9	54.7	−0.3	−0.4
(Arg 45) O	(Arg L92) NH1	3.3	87.9	−1.0	−0.4
(Arg 45) NH1	(Glu H50) OE1	2.8	44.5	−2.5	−5.3
(Arg 45) NH2	(Glu H35) OE1	4.9	57.5	−0.9	−2.8
(Asn 46) OD1	(Arg L92) NH2	2.5	39.0	*b*	−1.7
(Tyr 53) OH	(Trp H33) NE1	2.8	22.3	−0.4	1.0
(Gly 67) O	(Tyr H101) N	3.5	23.8	−0.4	−0.2
(Arg 68) NH1	(Glu H35) OE1	2.9	75.5	−3.7	−2.8
(Arg 68) NH2	(Glu H50) OE1	2.7	30.3	−3.2	−5.3
(Arg 68) NH2	(Glu H50) OE2	2.8	39.2	−3.7	−5.9

[a] Electrostatic energies listed for hydrogen bond donor groups (e.g., N–H H11–NH1–H12, etc.) are sums for all atoms of the group. Energy listed for carbonyl oxygen is the sum of contributions by atoms C and O. [b] Note the very short OD1–NH2 distance, 2.5 Å. Energy estimate is uncertain, but the actual listed energy contribution is repulsive (≈2 kcal).

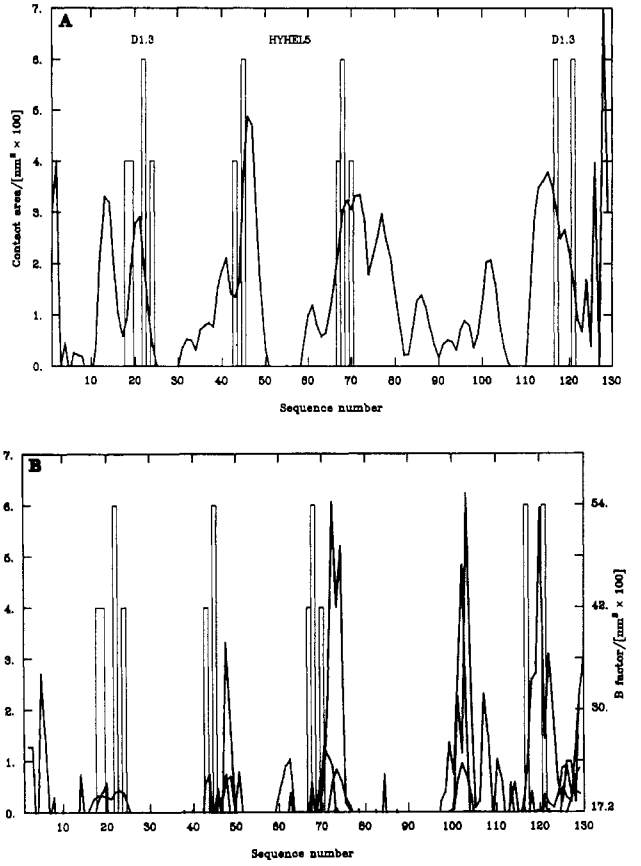

FIGURE 8: (A) Energetic epitopes of the lysozyme surface compared to the large probe accessibility profile computed as described before. Briefly, a spherical probe, comparable in size to immunoglobulin domains (radius 1 nm), is rolled over the lysozyme surface to identify its most protruding regions. The raw large probe contact surface data are smoothed and plotted as in the figure. The tall bars denote locations of lysozyme residues Gly 22, Gly 117, and Gln 121 (the D1.3 epitope) and Arg 45 and Arg 68 (the HyHEL-5 epitope). The short bars denote locations of residues that provide additional binding energy, namely, Asp 18, Ser 24, The 43, Gly 67, and Pro 70 (cf. Tables V and VIII). (B) Energetic epitopes of the lysozyme surface compared to average backbone *B* factors. Four different crystal structures served as sources of the *B* factors, namely, the human lysozyme (Artymiuk & Blake, 1981), the monoclinic hen egg white structure (Rao et al., 1983), the high-temperature structure of Berthou et al. (1983), and the hen egg white lysozyme of the HyHEL-5 complex (Sheriff et al., 1987). Note that segments with above-average backbone *B* factors often have different locations in the different structures. For example, the HyHEL-5 lysozyme profile has only two small, insignificant maxima between residues 15–25 and 125–130. Thus, biophysical significance of above-average backbone *B* factors remains unclear (Petsko & Ringe, 1984).

relative free energy contributions of Arg 45 and Arg 68 listed in Table VIII: that is, the Arg 45 contributes about 2.5 kal (≈10 kJ) less binding energy than the Arg 68. Figure 7 shows the energetically defined lysozyme HyHEL-5 epitope (i.e., the two residues Arg 68 and Arg 45) as the most protruding parts of that region of lysozyme surface. As was the case with the D1.3 antibody, this energetic epitope represents but a smaller part (some 30%) of the total antibody-contacting area.

Essential Attributes of Protein Antigenicity. In this paragraph, we discuss results of our calculations from the point of view of the following alternative concepts of antigenicity: (1) only a few discrete patches of protein surface are antigenic (Atassi, 1975, 1978); (2) essentially the whole protein surface is antigenic (Benjamin et al., 1984; Berzofsky, 1985); (3) backbone segmental flexibility is essential (Westhof et al., 1984; Tainer et al., 1985); (4) surface protrusion, as measured by the large probe accessibility algorithm (Novotny et al., 1986a), molecular cartography (Fanning et al., 1986), or idealized surface representations (Thornton et al., 1986), is essential.

Figure 8A shows both the large probe accessibility profile for the lysozyme (Novotny et al., 1986a) and locations of the D1.3 and HyHEL-5 energetic epitopes (cf. Tables V and VIII). The most essential residues of these two epitopes (Gly 22, Arg 45, Arg 68, Gly 117, and Gln 121) coincide with the most prominent peaks of the profile, supporting the large probe accessibility concept of antigenicity. The additional five residues that are listed in Tables V and VIII as contributing actively toward complex formation (Asp 18, Ser 24, Thr 43, Gly 67, and Pro 70) likewise cluster in surface regions that are convex. It has been noted that the most protruding residues are, by the nature of protein folds, mostly polar and electrically charged (Rose et al., 1985a; Geysen et al., 1987). Such side chains are most likely to contribute decisive enthalpic (electrostatic) stabilization of antigen–antibody complexes. Thus, the profile shown in Figure 8A can be interpreted as a probability profile, of various sequence segments, to contribute significantly toward complex formation with the antibody. In this model of antigenicity, certain parts of the protein surface are much more antigenic than others.

Intimate antigen–antibody contact brought about by favorable interactions between the small energetic epitope and the antigen binding site results in a contact area larger than that formed between the epitope and the site. For complex formation to be possible, the additional contact surfaces of the antibody and the antigen must be complementary to each other. If parts of this additional surface change shape and disrupt the complementarity, e.g., via amino acid substitutions in homologous cross-reacting proteins, a weaker affinity may be detected even if the energetic epitope remains intact. Experimental approaches sensitive to this phenomenon will

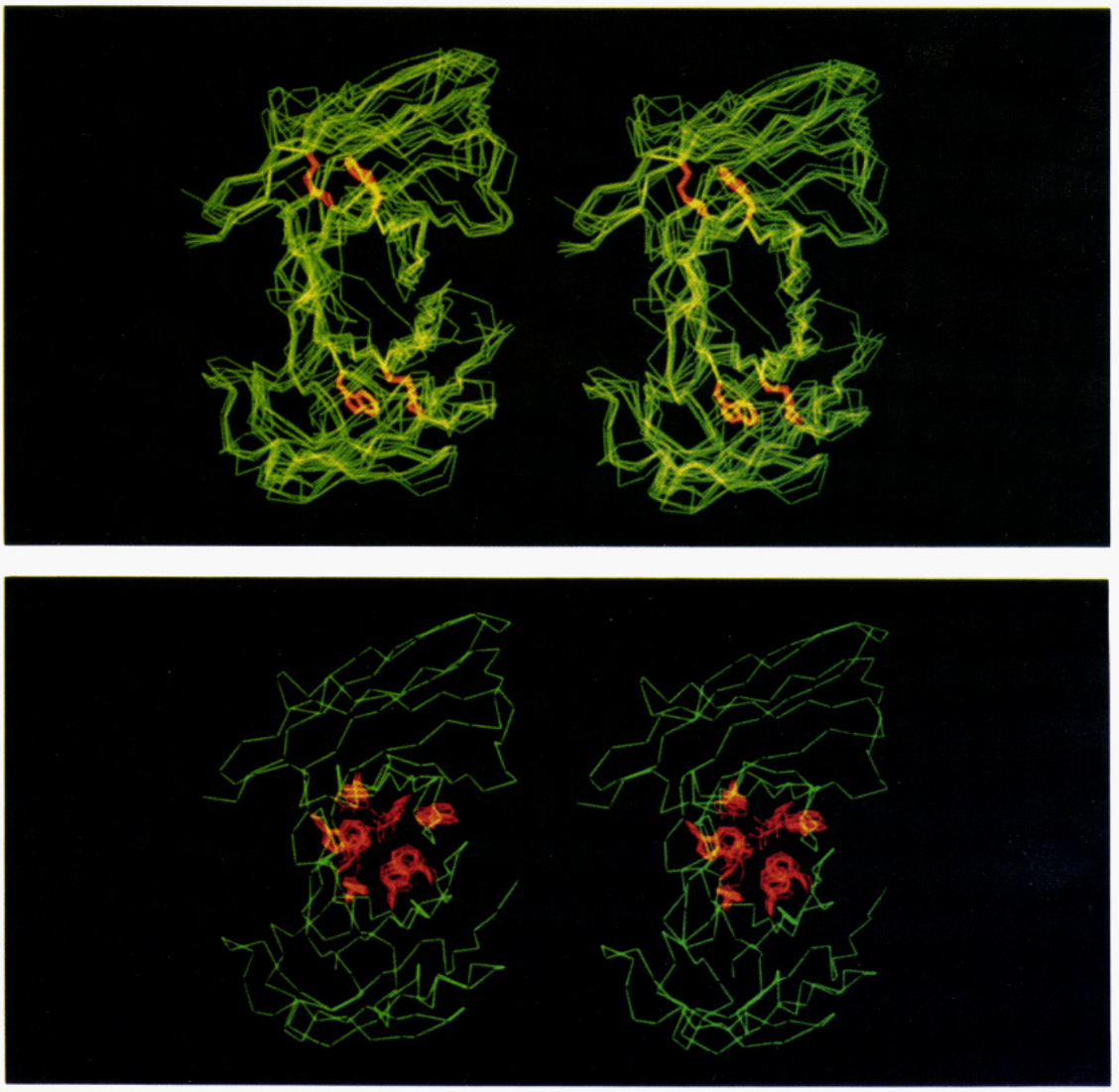

FIGURE 9: (A, top) Superposition of KOL, McPC 603, J539, NEW, HyHEL-5, and D1.3 VL and VH domains. By use of the program CONGEN, two side chains in each domain were least-squares superimposed on the corresponding side chains from the domain of the reference structure (KOL). The side chains, shown in red, are the invariant residues Cys 23, Cys 88, and Trp 35 (in the VL domains) or Cys 22, Cys 92, and Trp 36 (in the VH domains). Polypeptide backbones (green lines) are traced by Cα carbon atoms. Note that polypeptide chain segments involved in the VL–VH interface overlay virtually exactly despite the fact that the VL and VH domains were matched independently on their KOL counterparts, and no attempt was made to reproduce the extract mode of domain–domain association. (B, bottom) Carbon tracing of a Fv fragment showing residues important in mediating the VH–VL domain interaction. Residues shown from the six structures were not mutually superimposed; rather, the fit was produced as described in (A). The six aromatic rings at the interface are Tyr L36, Tyr L87, Phe L98, Trp H47, Tyr H91, and Trp H103 (Kabat et al. numbering). The two forked side chains at the bottom of the binding β-barrel are glutamines L38 and H39.

attribute antigenic properties to a large surface area, perhaps concluding that the whole protein surface is antigenic. Hence we arrive at different operational definitions of antigenicity, depending on whether we emphasize energetics of complex formation or complementarity of antigen–antibody surfaces. The accessibility concept of antigenicity identifies residues that are critical (i.e., most antigenic) from the energetic point of view. It also provides a link between the two extremes (distinct antigenic epitopes exist versus the whole surface is antigenic), by introducing the concept of antigenic probability that varies along the surface.

Figure 8B shows locations of average backbone Debye–Waller factors (crystallographic *B* factors) and the D1.3 and HyHEL-5 energetic epitopes. The *B* factor averages have often been interpreted as correlating directly with backbone segmental flexibility (Westhof et al., 1984; Tainer et al., 1984). Figure 8B shows that the energetically important residues rarely occur on these exceptionally flexible parts of the backbone. To explain this phenomenon, we envision that a certain amount of entropy (ΔS_{BB}) associated with flexible backbone segments becomes lost as the antigen–antibody complex is formed, and a corresponding $T\Delta S_{BB}$ factor has to be subtracted from the active Gibbs energy contributions. In exceptionally flexible segments, this factor may become a significant "force" directed against complex formation (Novotny et al., 1987).

Conformational Changes in Antibody Molecules upon Antigen Binding. The possible role of antibody conformational changes in complex formation has recently attracted much attention (Davies et al., 1988; Colman, 1988). The X-ray structure of the antibody–neuraminidase complex at 3-Å resolution (Colman et al., 1987) has been interpreted as indicating significant departures from the characteristic "canonical" pattern of VL–VH domain association, although this interpretation will probably be revised when the X-ray refinement is completed (Colman, 1988). The VL–VH dimerization pattern, based on the "perpendicular" noncovalent interaction of aromatic rings and a pair of hydrogen-bonded

Table X: Geometry of Domain–Domain Interface β-Sheets[a]

structure	semiaxis		helical pitch	twist angle, top to bottom	goodness of fit[b]
	major	minor			
KOL	1.01	0.65	4.19	214	0.140
McPC 603	1.08	0.66	4.24	220	0.132
NEW	1.07	0.63	4.33	210	0.150
J539	1.07	0.64	4.21	218	0.137
D1.3	1.05	0.65	4.21	225	0.123
HyHEL-5	0.98	0.65	4.27	210	0.129
REI (VL–VL)	0.99	0.68	4.27	204	0.124
av	1.03 ± 0.04	0.65 ± 0.02	4.25 ± 0.05	214 ± 7	0.134

[a] Dimensions are given in nanometers and angles in degrees. [b] Root-mean-square difference between the least-squares fitted strophoid surface and the backbone atoms N, Cα, and C.

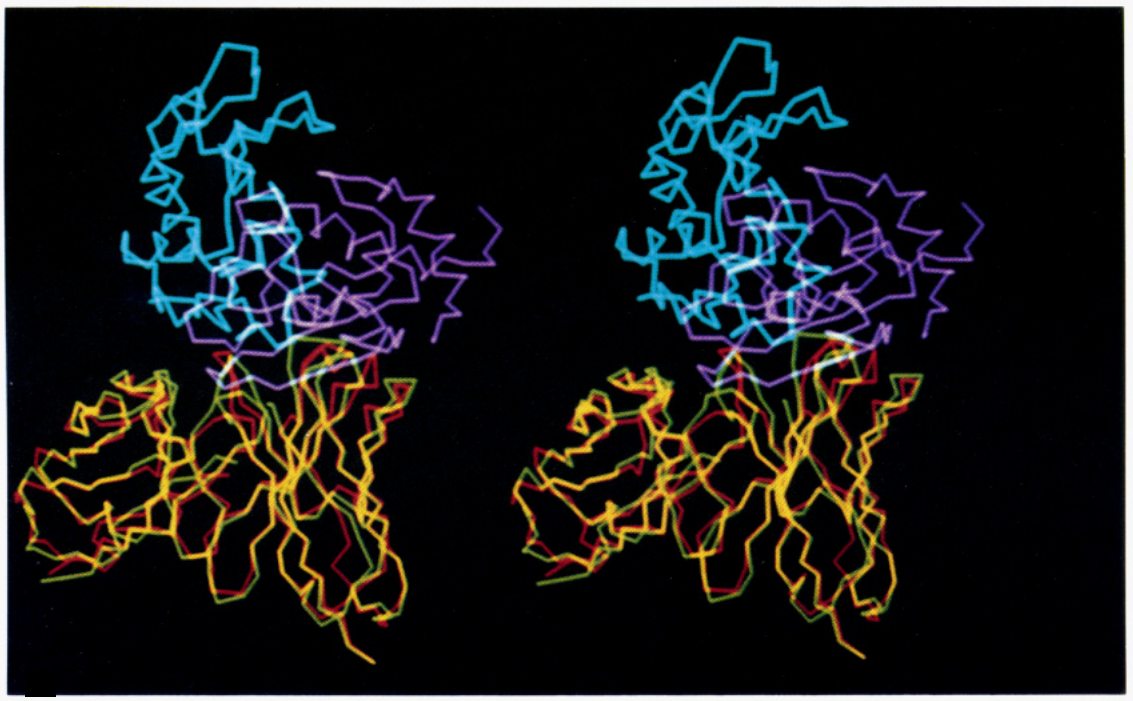

FIGURE 10: Stereo diagram of the two antibody–lysozyme complexes, D1.3 and HyHEL-5, least-squares superimposed. Only the Fv fragments were superimposed, and polypeptide backbones are shown as α-carbon tracings. The color coding is as follows: red and magenta, the HyHEL-5 Fv fragment and lysozyme, respectively; green and cyan, the D1.3 Fv fragment and lysozyme, respectively. Note that closely matching segments of the Fv backbones appear yellow, due to the red and green colors overlapping.

Gln residues, was previously identified as unique to the combining sites of antibodies (Novotny & Haber, 1985) and T-cell receptors (Novotny et al., 1986b). The β-sheet geometry associated with this type of domain–domain interaction was found to be exceptional and strictly conserved among immunoglobulins (Chothia et al., 1985; Novotny & Haber, 1985). We decided to analyze all the available crystallographic data for an indication of structural differences affecting the VH–VL domain association pattern.

Three independent approaches were used to assess structural similarities of the VL–VH interfaces. First, we used our geometrical model of a twisted hyperboloid (Novotny & Haber, 1985) to approximate the dimensions of the VH–VL interface β-barrel in different antibodies. Second, the two most conserved side chains of the VH and VL domains of all the Fv fragments [disulfide 22–36 and Trp 92 of the heavy chain, disulfide 23–88 and Trp 35 of the light chain in Kabat et al. (1987) numbering] were superimposed, for each domain independently, on a master VH–VL dimer to see whether the VL–VH interface geometry is independently conserved. Third, Fv fragments of the two Fv–lysozyme structures were least-squares superimposed.

Table X lists the essential geometrical parameters of the least-squares hyperboloid fit into the interface β-barrel. Virtually identical dimensions were found for all the six Fv fragments studied. Note that three of those, namely, KOL, NEW, and J539, are unliganded antibodies, while the three others, namely, D1.3, McPC603, and HyHEL-5, come from antibody–antigen complexes. Figure 9 depicts results of matching the Cys and Trp residues, independently and in all the VH and VL domains, with those of the "master" Fv structure of KOL. Once again, the geometry of the interface β-barrel is well preserved, and the conserved residues of the VH–VL interface, deemed to be essential for the domain–domain interaction (the pair of glutamines and the aromatic cluster), are found adopting very similar conformations. Finally, Figure 10 shows the results of the least-squares superposition of the Fv fragments D1.3 and HyHEL-5. The rms shift between backbone atoms of these two structures is 1.9 Å, including all the hypervariable loops. In the first approximation, backbones of the inner β-sheets are well conserved. It thus appears that the bottom part of the binding region, where many energetically important residues are found, has conserved backbone in the six structures studied.

Concluding Remarks

The calculated Gibbs free energy changes provide good initial estimates for relative binding contributions of individual

structural parts (side chains, domains, etc.) of antibodies and antigens, to the extent that these are known from experiments. The relative balance of the most important Gibbs free energy contributions, viz., the hydrophobic effect, electrostatic interactions, conformational entropy changes, and implicit solvent effects, also satisfies the expectations. The measured absolute ΔG values of antibody–ligand complexes have been matched by calculations in the cases of McPC 603 and D1.3 but not in the case of HyHEL-5, where calculations suggest an affinity greater than the current experimental value. Nevertheless, the agreement between the measured and calculated K_{AS} of the McPC 603 Fv–phosphocholine complex is of interest, inasmuch as this structure represents the simplest and the best characterized complex and is known to undergo no conformational changes on ligand binding.

Although our minimal free energy model (eq 2–7) appears to be approximately correct, the present work has helped to identify its weakest parts where future improvements will be needed most: (a) One is the electrostatic distance-dependent equation; a more realistic treatment, such as, e.g., the linearized Poisson equation, is called for. For example, the most important source of error in the case of the ΔG estimate for HyHEL-5 may well be the approximate nature of the electrostatic model. (b) More accurate estimates of conformational entropy changes are needed, e.g., uniform sampling of side-chain conformational space in the complex and in the free components. (c) Better estimates for the translational/rotational entropy loss should be attempted.

Overall, and as is often the case in modeling, we do better with relative properties than absolute. Our most important results relating to relative structural and energetic importance of individual residues can be summarized as follows.

Contact areas in Fv–lysozyme complexes are large, but productive binding appears to be mediated by a smaller number of residues, no more than five to six in both the Fv and the lysozyme antigen. The bottom part of the antigen binding cavity seems to be particularly important. This productive binding site surface covers some 65% of the total contact surface in both antibody–lysozyme complexes.

The energetically most important residues on the lysozyme surface define an energetic epitope. In the D1.3 epitope, the dominant Gibbs free energy contributions come from Gly 22, Gly 117, and Gln 121. In the HyHEL-5 epitope, the antibody affinity is largely determined by Arg 45 and Arg 68. The surface of the energetic epitopes is 2.5–3 nm^2, i.e., some 30% of the total lysozyme contact surface in both complexes. The residues constituting the energetic epitope belong to the most protruding parts of lysozyme surface and do not coincide with major maxima of the average backbone B factors obtained from crystallographic data. In addition to active, attractive contributions mediated by the energetic antigenic epitope, the "passive" surface complementarity is obviously an important factor.

The geometry of the binding region (i.e., the VH–VL interface β-sheet and the adjacent end points of hypervariable loops) is well conserved in all the six Fv fragment structures available. Three of these structures come from free Fab fragments while the three others are parts of liganded antibodies; it thus seems that major domain–domain rearrangements upon antigen binding ("domain slippages") are rare, if they occur at all.

Acknowledgments

We thank Drs. Michael Gilson (Columbia University), Barry Honig (Columbia University), Roy Mariuzza (Pasteur Institute), and Sandra Smith-Gill (NIH) for their kind communication of results prior to publication and for their discussion of our results. We also thank Drs. Simon E. V. Phillips and Ilya I. Haneef (Leeds University) for many valuable suggestions and Drs. Pedro Alzari and Roberto Poljak (Pasteur Institute, Paris) for critical comments. We are particularly obliged to Dr. Steven Sheriff (Squibb Institute) for his careful reading of the manuscript, his many helpful suggestions, and his insightful criticism.

Registry No. Phosphocholine, 107-73-3; lysozyme, 9001-63-2.

References

Alzari, P. M., Lascombe, M. B., & Poljak, R. J. (1988) *Annu. Rev. Immunol. 6*, 555–580.

Amit, A. G., Mariuzza, R. A., Phillips, S. E. V., & Poljak, R. (1986) *Science 233*, 747–752.

Artymiuk, P. J., Blake, C. C. F., Grace, D. E. P., Oatley, S. J., Phillips, D. C., & Sternberg, M. J. E. (1979) *Nature 280*, 563–568.

Atassi, M. Z. (1975) *Immunochemistry 12*, 423–438.

Atassi, M. Z. (1978) *Immunochemistry 15*, 909–936.

Atkins, P. W. (1978) *Physical Chemistry*, W. H. Freeman, San Francisco.

Bash, P. A., Singh, U. C., Brown, F. K., Langridge, R., & Kollman, P. A. (1987) *Science 235*, 574–576.

Benedetti, E., Morelli, G., Nemethy, G., & Scheraga, H. A. (1983) *Int. J. Pept. Protein Res. 22*, 1–15.

Benjamin, D. C., Berzofsky, J. A., East, I. J., Gurd, J. G., Miller, A., Prager, E. M., Reichlin, M., Sercarz, E. E., Smith-Gill, S. J., Todd, P. E., & Wilson, A. C. (1984) *Annu. Rev. Immunol. 2*, 67–101.

Berendsen, H. J. C., Postma, J. P. M., diNiola, A., van Gunsteren, W. F., & Haak, J. R. (1981) *J. Chem. Phys. 81*, 3684–3690.

Bernstein, F. C., Koetzle, T. F., Williams, G. J. B., Meyer, E. F., Brice, M. D., Rodgers, J. R., Kennard, O., Shimanouchi, T., & Tasumi, M. J. (1977) *J. Mol. Biol. 112*, 535–542.

Berthou, J., Lifshitz, Artymiuk, P., & Jolles, P. (1983) *Proc. R. Soc. London 217B*, 471–489.

Berzofsky, J. A. (1985) *Science 229*, 932–940.

Brooks, B., Bruccoleri, R. E., Olafson, B., States, D. J., Swaminathan, S., & Karplus, M. (1983) *J. Comput. Chem. 4*, 187–217.

Bruccoleri, R. E., & Karplus, M. (1987) *Biopolymers 26*, 137–168.

Bruccoleri, R. E., Novotny, J., Keck, P., & Cohen, C. (1986) *Biophys. J. 49*, 79–81.

Burley, S. K., & Petsko, G. A. (1985) *Science 229*, 3–28.

Chothia, C. (1974) *Nature 248*, 338–339.

Chothia, C., & Janin, J. (1975) *Nature 256*, 705–708.

Chothia, C., Novotny, J., Bruccoleri, R. E., & Karplus, M. (1985) *J. Mol. Biol. 186*, 651–663.

Colman, P. (1988) *Adv. Immunol.* (in press).

Colman, P. M., Laver, W. G., Varghese, J. N., Baker, A. T., Tulloch, P. A., Air, G. M., & Webster, R. G. (1987) *Nature 326*, 358–363.

Davies, D. R., Sheriff, S., & Padlan, E. A. (1988) *J. Biol. Chem. 263*, 10541–10544.

Deisenhofer, J. (1981) *Biochemistry 20*, 2361–2370.

Eisenberg, D., & Kautzmann, W. (1969) in *Structure and Properties of Water*, pp 79–81, Oxford University Press, New York.

Eisenberg, D., & McLachlan, A. D. (1986) *Nature 319*, 199–203.

Fanning, W. E., Smith, J. A., & Rose, D. G. (1986) *Biopolymers 25*, 863–883.

Fersht, A. R., Shi, J. P., Knill-Jones, J., Lowe, D. M., Wilkinson, J., Blow, D. M., Brick, P., Carter, P., Waye, M. Y., & Winer, G. (1985) *Nature 314*, 235–238.

Gelin, B., & Karplus, M. (1979) *Biochemistry 18*, 1256–1268.

Geysen, H. M., Tainer, J. A., Rodda, S. J., Mason, T. J., Alexander, H., Getzoff, E. D., & Lehrner, R. A. (1987) *Science 235*, 1184–1190.

Gilson, M., & Honig, B. (1987) *Nature 330*, 84–86.

Gilson, M., & Honig, B. (1988a) *Proteins 3*, 32–52.

Gilson, M., & Honig, B. (1988b) *Proteins 4*, 7–18.

Grossberg, A. L., Krausz, L. M., Rendina, L., & Pressman, D. (1974) *J. Immunol. 113*, 1807.

Hagler, A. (1984) in *Molecular Dynamics and Protein Structure* (Hermans, J., Ed.) pp 133–139, Western Springs, IL.

Harper, M., Lema, F., Boulot, G., & Poljak, R. J. (1987) *Mol. Immunol. 24*, 97–108.

Hodges, R. S., Heaton, R. J., Parker, J. M. R., Molday, L., & Molday, R. S. (1988) *J. Biol. Chem. 263*, 11768–11775.

Huber, R., Kukla, D., Bode, W., Schwager, P., Barterls, K., Deisenhofer, J., & Steigemann, W. (1974) *J. Mol. Biol. 89*, 73–101.

James, M. N. G., & Sielecki, A. R. (1983) *J. Mol. Biol. 163*, 299–361.

Jencks, W. P. (1981) *Proc. Natl. Acad. Sci. U.S.A. 78*, 4046–4050.

Kabat, E. A. (1970) *Ann. N.Y. Acad. Sci. 169*, 43–54.

Kabat, E. A., Wu, T. T., Reid-Miller, M., Perry, H. M., & Gottesman, K. S. (1987) in *Sequences of Proteins of Immunological Interest*, Public Health Service, National Institutes of Health, Bethesda, MD.

Kauzmann, W. (1959) *Adv. Protein Chem. 14*, 1–64.

Lavoie, T. B., Kam-Morgan, L. N. W., Hartman, A. B., Sheriff, S., Saroff, D. G., Mainhart, C. R., Hamel, P., Kirsh, J. F., Wilson, A., & Smith-Gill, S. J. (1989) in *The Immune Response to Structurally Defined Proteins: the Lysozyme Model*, Adenine Press, New York (in press).

Lee, B. K., & Richards, F. M. (1971) *J. Mol. Biol. 119*, 537–555.

Levitt, M., & Lifson, S. (1969) *J. Mol. Biol. 46*, 269–279.

Lumry, R., & Biltonen, R. (1969) in *Structure and Stability of Biological Macromolecules* (Timasheff, S. N., & Fasman, G. D., Eds.) Marcel Dekker, New York.

Mariuzza, R. A., Phillips, S. E. V., & Poljak, R. J. (1987) *Annu. Rev. Biophys. Biophys. Chem. 16*, 139–160.

Marquart, M., Deisenhofer, J., Huber, R., & Palm, W. (1980) *J. Mol. Biol. 141*, 369–391.

Matsumura, M., Becktel, W. J., & Matthews, B. W. (1988) *Nature 334*, 406–410.

McCammon, J. A., Karim, O. A., Lybrand, T. P., & Wong, C. F. (1986) *Ann. N.Y. Acad. Sci. 482*, 210–221.

McGregor, M. J., Islam, S. A., & Sternberg, M. J. E. (1987) *J. Mol. Biol. 198*, 295–310.

Mehler, E. L., & Eichele, G. (1984) *Biochemistry 23*, 3887–2891.

Mezei, M., & Beveridge, D. L. (1986) *Ann. N.Y. Acad. Sci. 482*, 1–23.

Mukkur, T. K. S. (1984) *CRC Crit. Rev. Biochem. 16*, 133–167.

Nemethy, G., Pottle, M. S., & Scheraga, H. A. (1983) *J. Phys. Chem. 87*, 1883–1887.

Novotny, J., & Haber, E. (1985) *Proc. Natl. Acad. Sci. U.S.A. 82*, 4592–4596.

Novotny, J., Bruccoleri, R. E., & Newell, J. (1984) *J. Mol. Biol. 177*, 567–573.

Novotny, J., Handschumacher, M., Haber, E., Bruccoleri, R. E., Carlson, W. B., Fanning, D. W., Smith, J. A., & Rose, G. D. (1986a) *Proc. Natl. Acad. Sci. U.S.A. 83*, 226–230.

Novotny, J., Tonegawa, S., Saito, H., Kranz, D. M., & Eisen, H. N. (1986b) *Proc. Natl. Acad. Sci. U.S.A. 83*, 742–746.

Novotny, J., Handschumacher, M., & Bruccoleri, R. E. (1987) *Immunol. Today 8*, 26–31.

Nozaki, Y., & Tanford, C. (1971) *J. Biol. Chem. 246*, 2211–2217.

Ooi, T., Oobatake, M., Nemethy, G., & Scheraga, H. A. (1987) *Proc. Natl. Acad. Sci. U.S.A. 84*, 3086–3090.

Padlan, E. A., Davies, D. R., Rudikoff, S., & Potter, M. (1976) *Immunochemistry 13*, 945–949.

Page, M. I., & Jencks, W. P. (1971) *Proc. Natl. Acad. Sci. U.S.A. 68*, 1678–1683.

Petsko, G., & Ringe, D. (1984) *Annu. Rev. Biophys. Bioeng. 13*, 331–372.

Pettitt, B. M., & Karplus, M. (1985) *J. Chem. Phys. 83*, 781–789.

Poljak, R. J., Amzel, L. M., Avey, H. P., Chen, B. L., Phizackerley, R. P., & Saul, F. (1973) *Proc. Natl. Acad. Sci. U.S.A. 70*, 3305–3310.

Ponder, J. W., & Richards, F. M. (1987) *J. Mol. Biol. 193*, 775–791.

Privalov (1979) *Adv. Protein Chem. 33*, 167–241.

Quiocho, F. A., Sack, J. S., & Vyas, N. K. (1987) *Nature 329*, 561–564.

Rao, S. T., Hogle, J., & Sundaralingam, M. (1983) *Acta Crystallogr. C39*, 237–283.

Rashin, A. A. (1984) *Biopolymers 23*, 1605–1620.

Rashin, A. A., & Namboodiri, K. A. (1987) *J. Phys. Chem. 91*, 6003–6012.

Reiher, W. (1985) Ph.D. Thesis, Harvard University.

Rose, G. D., Gierash, I. M., & Smith, J. A. (1985a) *Adv. Protein Chem. 37*, 1.

Rose, G. D., Geselowitz, A. R., Lesser, G. J., Lee, R. H., & Zehfus, M. H. (1985b) *Science 229*, 834–838.

Ross, P. D., & Subramanian, S. (1981) *Biochemistry 20*, 3096–3102.

Rossky, P. J. (1986) *Ann. N.Y. Acad. Sci. 482*, 91–114.

Rudikoff, S., Potter, M., Segal, D. M., Padlan, E. A., & Davies, D. R. (1972) *Proc. Natl. Acad. Sci. U.S.A. 66*, 3689–3692.

Satow, Y., Cohen, G. H., Padlan, E. A., & Davies, D. R. (1986) *J. Mol. Biol. 190*, 593–604.

Saul, F. A., Amzel, L. M., & Poljak, R. J. (1978) *J. Biol. Chem. 253*, 585–597.

Schechter, I. (1971) *Ann. N.Y. Acad. Sci. 190*, 394–419.

Segal, D., Padlan, E. A., Cohen, G. H., Rudikoff, S., Potter, M., & Davies, D. R. (1974) *Proc. Natl. Acad. Sci. U.S.A. 71*, 4298–4302.

Sela, M. (1969) *Science 166*, 1365–1374.

Sheriff, S., Silverton, E. W., Padlan, E. A., Cohen, G. H., Smith-Gill, S. J., Finzel, B. C., & Davies, D. R. (1987) *Proc. Natl. Acad. Sci. U.S.A. 84*, 8075–8079.

Singh, U. C., & Kollman, P. A. (1984) *J. Comput. Chem. 5*, 129–303.

Skerra, A., & Pluecktthurn, A. (1988) *Science 240*, 1038–1041.

Smith-Gill, S. J., Wilson, A. C., Potter, M., Prager, E. M., Feldmann, R. J., & Mainhart, C. R. (1982) *J. Immunol. 128*, 314–322.

Sternberg, M. J. E., Hayes, F. R. F., Russell, A. J., Thomas, P. G., & Fersht, A. R. (1987) *Nature 330*, 86–88.

Suh, S. W., Bhat, T. N., Navia, M. A., Cohen, G. H., Rao, D. N., Rudikoff, S., & Davies, D. R. (1986) *Proteins 1*, 74–80.
Summers, N., Carlson, W., & Karplus, M. (1987) *J. Mol. Biol. 196*, 175–198.
Szebenyi, D. M. E., & Moffat, K. (1986) *J. Biol. Chem. 261*, 8761–8777.
Tainer, J. A., Getzoff, E. D., Alexander, H., Houghten, R. A., Olson, A. J., Lerner, R. E., & Hendrickson, W. A. (1984) *Nature 312*, 127–134.
Tainer, J., Getzoff, E. D., Paterson, Y. A., Olson, A. J., & Lerner, R. A. (1985) *Annu. Rev. Immunol. 3*, 501–535.
Thornton, J. M., Edwards, M. S., Taylor, W. R., & Barlow, D. J. (1986) *EMBO J. 5*, 409–413.
Verhoeyen, M., Milstein, C., & Winter, G. (1988) *Science 239*, 1534–1536.
Warshel, A., & Levitt, M. (1976) *J. Mol. Biol. 103*, 227–249.
Warshel, A., Sussman, F., & King, G. (1986) *Biochemistry 25*, 8368–8372.
Warwicker, J. (1986) *J. Theor. Biol. 121*, 199–210.
Weber, G. (1975) *Adv. Protein Chem. 29*, 2–84.
Weiner, P. K., & Kollman, P. A. (1981) *J. Comput. Chem. 2*, 287–303.
Weiner, S. J., Kollman, P. A., Case, D. A., Singh, U. C., Ghio, C., Alagona, G., Profeta, S., & Weiner, P. (1984) *J. Am. Chem. Soc. 106*, 765–784.
Westhof, E., Altschuh, D., Moras, D., Bloomer, A. C., Mondragon, A., Klug, A., & Regenmortel, M. H. V. (1984) *Nature 311*, 123–126.
Whitlow, M., & Teeter, M. M. (1986) *J. Am. Chem. Soc. 108*, 7163–7172.
Williams, D. E. (1980) *Acta Crystallogr. A36*, 715.
Xu, G. J., & Weber, G. (1982) *Proc. Natl. Acad. Sci. U.S.A. 79*, 5268–5271.

Identification of Lung Major GTP-Binding Protein as G_{i2} and Its Distribution in Various Rat Tissues Determined by Immunoassay†

Tomiko Asano,*,‡ Rika Morishita,‡ Reiji Semba,‡ Hiroshi Itoh,§ Yoshito Kaziro,§ and Kanefusa Kato‡

Institute for Developmental Research, Kasugai, Aichi 480-03, Japan, and Institute of Medical Science, University of Tokyo, 4-6-1, Shirokanedai, Minatoku, Tokyo 108, Japan

Received November 16, 1988; Revised Manuscript Received February 16, 1989

ABSTRACT: Antisera were raised in rabbits against the 40-kDa α subunit of bovine lung GTP-binding protein, which were identified as the α subunit of G_{i2} ($G_{i2}\alpha$) by the analysis of the partial amino acid sequence. Antibodies were purified with a $G_{i2}\alpha$-coupled Sepharose column and then were passed through a $G_{i1}\alpha$-coupled Sepharose column to remove antibodies reactive also with 41-kDa α. Purified antibodies reacted with $G_{i2}\alpha$, but not with $G_{i1}\alpha$, $G_{i3}\alpha$, or $G_o\alpha$ in an immunoblot assay. A sensitive enzyme immunoassay method for the quantification of $G_{i2}\alpha$ was developed by using these purified antibodies. The assay system consisted of polystyrene balls with immobilized antibody $F(ab')_2$ fragments and the same antibody Fab' fragments labeled with β-D-galactosidase from *Escherichia coli*. The minimal detection limit of the assay was 1 fmol, or 40 pg. Samples from various tissues were solubilized with 2% sodium cholate and 1 M NaCl, and the concentrations of $G_{i2}\alpha$ were determined. $G_{i2}\alpha$ was detected in all the tissues examined in the rat. The highest concentration was found in platelets and leukocytes when the data were expressed as picomoles per milligram of protein. The spleen, lung, and cerebral cortex contained relatively high levels of $G_{i2}\alpha$. In the bovine brain, $G_{i2}\alpha$ was distributed almost uniformly among the various regions. The concentrations of $G_{i2}\alpha$ were constant in the rat brain throughout ontogenic development, in contrast with those of $G_o\alpha$ which were markedly increased with age.

Among the GTP-binding proteins (G proteins),[1] there are several proteins which can be ADP-ribosylated by pertussis toxin. They include transducin, G_i, and G_o, which are known to be homologous proteins (Gilman, 1987). Transducin is localized in the vertebrate retina and communicates between light activation of rhodopsin and stimulation of cyclic GMP phosphodiesterase. G_o is predominantly localized in nervous tissues and neuroendocrine cells (Sternweis & Robishaw, 1984; Asano et al., 1988c). The functions of G_i and G_o are not fully elucidated yet, but evidence suggests that they are involved not only in inhibition of adenylate cyclase but also in stimulation of phospholipase C and phospholipase A_2 (Gilman, 1987). Some other reports indicate that the K^+ channel or Ca^{2+} channel is regulated by G_i, G_o, or other G proteins. These G proteins are composed of three different subunits, α, β, and γ. The α subunit is unique to each G protein, while the β and γ subunits are considered to be identical with or very similar

† This work was supported in part by a grant-in-aid for scientific research from the Ministry of Education, Science and Culture of Japan and by a research grant from the Ishida Foundation.
* Correspondence should be addressed to this author.
‡ Institute for Developmental Research.
§ Institute of Medical Science.

[1] Abbreviations: G protein, GTP-binding protein; G_i, inhibitory GTP-binding protein of adenylate cyclase; G_o, related GTP-binding protein of unknown function; Hepes, 4-(2-hydroxyethyl)-1-piperazineethanesulfonic acid; SDS–PAGE, sodium dodecyl sulfate–polyacrylamide gel electrophoresis; TPCK, tosylphenylalanyl chloromethyl ketone; kDa, kilodalton(s); Tris-HCl, tris(hydroxymethyl)aminomethane hydrochloride; EDTA, ethylenediaminetetraacetic acid.

0006-2960/89/0428-4749$01.50/0